

NASA TECHNICAL NOTE



NASA TN D-6753

a /

NASA TN D-6753

LOAN COPY: RETURN
AFWL (DOUL)
KIRTLAND AFB, N.

0133682



TECH LIBRARY KAFB, NM

HYPersonic AERODYNAMICS AND
ENTRY-MANEUVER—AEROTHERMODYNAMIC
INTERACTIONS FOR
TWO LIFTING ENTRY VEHICLES

by James P. Arrington and William C. Woods

*Langley Research Center
Hampton, Va. 23365*

NATIONAL AERONAUTICS AND SPACE ADMINISTRATION • WASHINGTON, D. C. • MAY 1972





0133682

1. Report No. NASA TN D-6753		2. Government Accession No.		3. Recipient's Catalog No.	
4. Title and Subtitle HYPERSONIC AERODYNAMICS AND ENTRY-MANEUVER — AEROTHERMODYNAMIC INTERACTIONS FOR TWO LIFTING ENTRY VEHICLES		5. Report Date May 1972		6. Performing Organization Code	
7. Author(s) James P. Arrington and William C. Woods		8. Performing Organization Report No. L-8072		10. Work Unit No. 117-07-01-01	
9. Performing Organization Name and Address NASA Langley Research Center Hampton, Va. 23365		11. Contract or Grant No.		13. Type of Report and Period Covered Technical Note	
12. Sponsoring Agency Name and Address National Aeronautics and Space Administration Washington, D.C. 20546		14. Sponsoring Agency Code		15. Supplementary Notes	
16. Abstract <p>The longitudinal, directional, and lateral static stability and control characteristics of a delta lifting body and a delta-wing body have been obtained at a Mach number of 20 in helium for operational Reynolds numbers over an angle-of-attack range of -4° to 55°. The aerodynamic characteristics of the wing body were then evaluated in an entry study to examine the effects of vehicle performance on the aerothermodynamic parameters associated with constant and variable angle-of-attack modes for a 1500-n.-mi. cross range.</p> <p>The experimental results indicated that the vehicles were stable, except for neutral directional stability for the wing-body shape, and could be trimmed over the operational angle-of-attack range; however, the wing-body vehicle had adverse yaw due to roll control. This roll-yaw coupling was not examined for the lifting body.</p> <p>The trajectory analysis indicated that a 17-percent decrease in performance required little change in the constant angle-of-attack entry mode and, in turn, resulted in a small decrease in the total heat load. For the pitch-modulated entry, the performance decrease required the pitch maneuver to begin earlier during entry and to last longer in order to meet the 1500-n.-mi. cross range without a major heating penalty. The performance reduction also had little effect on the maximum laminar radiation equilibrium temperature over a major portion of the lower surface of the wing-body vehicle regardless of the entry mode.</p>					
17. Key Words (Suggested by Author(s)) Space-shuttle hypersonic aerothermodynamics Lifting entry Entry-maneuver—aerothermodynamic interactions			18. Distribution Statement Unclassified — Unlimited		
19. Security Classif. (of this report) Unclassified		20. Security Classif. (of this page) Unclassified		21. No. of Pages 59	22. Price* \$3.00

HYPERSONIC AERODYNAMICS AND
ENTRY-MANEUVER—AEROTHERMODYNAMIC INTERACTIONS
FOR TWO LIFTING ENTRY VEHICLES

By James P. Arrington and William C. Woods
Langley Research Center

SUMMARY

The longitudinal, directional, and lateral static stability and control characteristics of two classes of lifting entry vehicles originally proposed for a reusable space-shuttle orbiter — a delta lifting body and a delta-wing body — have been obtained at a Mach number of 20 in helium for operational Reynolds numbers over an angle-of-attack range of -4° to 55° . The aerodynamic characteristics of the delta-wing body were then evaluated in an entry-analysis study to examine the effects of vehicle performance on the aerothermodynamic parameters associated with constant and variable angle-of-attack modes for a 1500-n.-mi. cross range.

The experimental results showed that the vehicles were stable, except for neutral directional stability for the delta-wing body, and could be trimmed over the operational angle-of-attack range; however, the wing-body vehicle had adverse yaw due to roll control. This roll-yaw coupling was not examined for the lifting body.

The trajectory analysis showed that a 17-percent decrease in performance required little change in the maneuvers for the constant angle-of-attack entry mode and, in turn, resulted in only a small decrease in total heat load. For the pitch-modulated entry, the decrease in performance required the pitch maneuver to begin earlier during entry and to last longer in order to meet the 1500-n.-mi. cross range without a major heating penalty. The reduction in performance also had little effect on the maximum laminar radiation equilibrium temperature over a major portion of the lower surface of the wing-body vehicle regardless of the entry mode.

INTRODUCTION

Past studies have been directed toward evaluating candidate space-shuttle concepts for a reusable transportation system capable of transferring large payloads to and from earth orbit. (See, for example, refs. 1, 2, and 3.) Preliminary trajectory analyses (ref. 4, for example) indicate that, in order to survive the thermal environment and to meet shuttle cross-range requirements, these vehicles must be capable of trimming at high angles of attack near maximum lift coefficients and at low angles of attack near maximum lift-drag ratios. In the present study, hypersonic wind-tunnel tests were con-

ducted on two early shuttle candidates – a delta planform lifting body and a delta-wing body – to determine if these two vehicle classes could meet these trim requirements with realistic center-of-gravity positions.

The static aerodynamic characteristics of these two classes of vehicles were experimentally evaluated at Mach numbers near 20 for operational Reynolds numbers. The data were obtained in the Langley 22-inch helium tunnel at angles of attack from -4° to 55° for sideslip angles of 0° and 4.5° . A portion of the wing-body-vehicle experimental characteristics and some calculated aerodynamics were applied to entry trajectories to evaluate the effect of performance on the entry maneuvers and the aerothermodynamic parameters associated with constant and variable angle-of-attack entry modes. Portions of this work were used for the aerodynamic inputs for the trajectory and heating analysis presented in reference 4.

Owing to the dynamic nature of the shuttle program, the external lines of candidate configurations have not remained fixed for any appreciable time period. The shuttle does have a high cross-range requirement and must survive the associated thermal environment; consequently, aerodynamic performance requirements have not changed appreciably. The present configurations, though no longer shuttle candidates, were designed to have these requirements; therefore, this analysis of aerothermodynamic interactions is representative of that associated with present shuttle concepts.

SYMBOLS

The longitudinal data are referred to both the body (C_N, C_A, C_m) and stability (C_L, C'_D) axis systems. Lateral and directional data are referred to the body axis system (fig. 1).

The units used for the physical quantities of this paper are given both in the International System of Units (SI) and in the U.S. Customary Units. Measurements and calculations were made in U.S. Customary Units.

C_A axial-force coefficient, $\frac{\text{Total axial force}}{qS}$

C_D C'_D at $\beta = 0^\circ$

C'_D drag coefficient, $C_A \cos \alpha + C_N \sin \alpha$

C_L lift coefficient, $C_N \cos \alpha - C_A \sin \alpha$

$C_{L,max}$ maximum lift coefficient

C_l	rolling-moment coefficient, $\frac{\text{Rolling moment}}{qS\ell}$
$C_{l\beta}$	rate of change of rolling-moment coefficient with sideslip angle, $\frac{\Delta C_l}{\Delta\beta}$, per degree
$C_{l\delta_a}$	rate of change of rolling-moment coefficient with aileron deflection angle, $\frac{\Delta C_l}{\Delta\delta_a}$, per degree
C_m	pitching-moment coefficient, $\frac{\text{Pitching moment}}{qS\ell}$
C_N	normal-force coefficient, $\frac{\text{Normal force}}{qS}$
C_n	yawing-moment coefficient, $\frac{\text{Yawing moment}}{qS\ell}$
$C_{n\beta}$	rate of change of yawing-moment coefficient with sideslip angle, $\frac{\Delta C_n}{\Delta\beta}$, per degree
$C_{n\delta_a}$	rate of change of yawing-moment coefficient with aileron deflection angle, $\frac{\Delta C_n}{\Delta\delta_a}$, per degree
C_Y	side-force coefficient, $\frac{\text{Side force}}{qS}$
$C_{Y\beta}$	rate of change of side-force coefficient with sideslip angle, $\frac{\Delta C_Y}{\Delta\beta}$, per degree
$C_{Y\delta_a}$	rate of change of side-force coefficient with aileron deflection angle, $\frac{\Delta C_Y}{\Delta\delta_a}$, per degree
h	altitude
L/D	lift-drag ratio, C_L/C_D
ℓ	body reference length
M	Mach number
Q	total heat load
q	dynamic pressure

\dot{q}	heating rate
R	Reynolds number based on body length
r	radius
S	reference planform area
T_e	maximum-radiation equilibrium temperature
t	time
V	velocity
W	weight
x	longitudinal coordinate measured from model nose (see fig. 2(a))
y	lateral coordinate measured from model center line (see fig. 2(a))
α	angle of attack, deg
β	sideslip angle, deg
γ_e	entry angle, deg
δ_a	aileron-deflection angle, $\frac{\delta_{e,left} - \delta_{e,right}}{2}$, deg
δ_b	body-flap deflection angle, positive down, deg
δ_e	elevon-deflection angle, positive when deflected down, $\frac{\delta_{e,left} + \delta_{e,right}}{2}$, deg
θ	tip-fin roll-out angle, deg
ϕ	bank angle measured about velocity vector, deg
ϕ_e	initial bank angle at entry
ϕ_f	final bank angle after pull-out

MODELS

The wing-body configuration was a 0.0036-scale version of the Martin Marietta Corporation entry vehicle examined in the integral launch and reentry vehicle (ILRV) study presented in reference 1. It had a double delta planform with a body leading-edge sweep of 82° and a wing leading-edge sweep of 67.5° . The nose was canted up at 6.7° , and the lower afterbody had a 10° boattail which extended out to the wing tips. The elevons and body flap were considered to be at zero deflection when positioned up at this 10° angle. (See fig. 2(a).) The tip fins were toed in 5° and were rolled out 13.5° , 15° , and 20° . The moments, taken about a point at 65.9 percent of the body length, used the body length (0.186 m, or 7.32 in.) as a reference. The reference area, 0.0092 m^2 (14.26 in^2), was the planform area of the body and wings without the tip fins.

A body fin was also evaluated for its effects on lateral and directional stability. The fin planform shape was similar to a wing-tip fin as shown in figure 2(b). Several body and wing cross sections are presented in figure 2(c).

The lifting-body configuration (fig. 3) was a 0.006-scale model of the Lockheed Missiles & Space Company ILRV entry vehicle designated LMSC 8MX in reference 2. The vehicle had a delta-body planform shape with a leading-edge sweep of 77.8° , nose canted up at 6° , and a 5° lower afterbody boattail. Relatively large elevons were used for longitudinal stability and control, and tip fins, toed in 5° and rolled out 30° , were used for lateral and directional stability. The moments, taken about a point at 72 percent of the reference length, used the length from the virtual origin of the delta planform to the elevon hinge line as the reference (0.150 m, or 5.9 in.). The reference area, 0.0049 m^2 (7.60 in^2), was the triangular area determined by the leading-edge sweep angle and the body reference length ($l^2 \cot 77.8^\circ$).

APPARATUS AND TESTS

Wind Tunnel

The experimental investigations were conducted in the Langley 22-inch helium tunnel. Operational characteristics of the facility and details of the contoured nozzle flow calibrations are available in reference 5.

Tests

All models were mounted on a sting-supported six-component strain-gage balance. Because of the limitation of the angle-of-attack mechanism, two sets of stings were required to cover the complete angle range. These stings and the test results using them are discussed in the appendix.

The angles of attack were set by using a prism mounted in the model to reflect light from a point (adjacent to the test-section window) onto a calibrated scale. Additional features of the system can be found in reference 5. Sideslip angles were obtained by changing the angle of attack of the model with the sting yawed at fixed angles of 0° and 4.5° . For the high angle-of-attack sideslip tests, the sting always came straight out of the model base.

The test Reynolds numbers based on model reference lengths were 1.28×10^6 at $M = 19$ for the lifting body and 1.5×10^6 at $M = 19$ and 2.9×10^6 at $M = 20.6$ for the wing body. The Reynolds number range resulted from changes in the stagnation pressure which also caused the small Mach number variation. In figure 4 the range of Mach numbers and Reynolds numbers that can be obtained in the facility is superimposed over Mach number—Reynolds number envelopes generated by shuttle (ILRV) candidates flying proposed entry trajectories (see, for example, refs. 1, 2, and 3).

The estimated maximum errors in the measured basic data and in the test conditions are shown for the two configurations in the following table:

	Lifting body	Wing body
C_N	± 0.023	± 0.007
C_A	± 0.006	± 0.002
C_m	± 0.003	± 0.0008
C_l	± 0.001	± 0.0003
C_n	± 0.001	± 0.0003
C_Y	± 0.008	± 0.002
α , deg	± 0.1	± 0.1
β , deg	± 0.1	± 0.1
$\delta_a, \delta_b, \delta_e$, deg	± 0.05	± 0.05
M	± 0.2	± 0.2

Uncertainties in the aerodynamic coefficients and the test parameters were determined from a static calibration of the balance, readout errors, and test-section Mach number calibrations. Base pressures were measured at one location on the sting throughout the low angle-of-attack range (0° to 20°), and the balance axial forces were adjusted to a condition in which free-stream pressure acted over the model base areas (minus the balance cross-sectional area).

RESULTS AND DISCUSSION

Aerodynamic Characteristics

Wing body.- Tests were conducted at two Reynolds numbers, 1.5×10^6 and 2.9×10^6 , which bound the range expected for space-shuttle vehicles at Mach numbers near 20 (fig. 4). The test at the higher Reynolds number had a lower skin-friction coefficient which resulted in a lower axial-force coefficient as shown in figure 5. The relatively small effects of this Reynolds number range on the other components are also indicated.

The effect of elevon deflections on the longitudinal aerodynamic characteristics of the wing-body configuration is presented in figures 6 to 8 for three tip-fin roll-out angles, 13.5° , 15° , and 20° . The data show that the vehicle could be trimmed with stable static stability from the $(L/D)_{\max}$ angle of attack near 16° up to the preliminary design entry angle of 45° with only about a 20° elevon change. Rolling the fins out from 13.5° to 20° reduced the required elevon deflection into the flow by 5° in order to trim near $(L/D)_{\max}$. The deflection could be further reduced by using a body flap in conjunction with the elevons as indicated by the comparison made with and without a body flap in figure 9.

A body fin was attached to the configuration with $\theta = 13.5^\circ$ and $\delta_e = 20^\circ$ (fig. 2(b)) in order to evaluate the hypersonic effects for this possible subsonic requirement. The data in figures 10 and 11 show that the fin affected only the aerodynamic characteristics for angles of attack less than 10° , which is below the hypersonic operational attitude range of the vehicle.

Directional and lateral static stability characteristics of the wing-body configuration are presented in figure 11 for control deflections required to trim at both the high and low angles of attack. The vehicle with $\theta = 13.5^\circ$ possessed lateral static stability over the test angle-of-attack range but had essentially neutral static directional stability. Increasing the tip-fin roll-out angle improved the directional stability as shown in figure 12. The data also show that elevon deflections had small effects on the lateral and directional characteristics.

The vehicle with $\theta = 13.5^\circ$ was evaluated for roll control by differentially deflecting the elevons ($\delta_a = 15^\circ$) about a 5° elevon deflection for trim at the higher angles of attack (fig. 13). The results in figure 14 show that this configuration developed adverse yaw due to roll control. Although directional stability and yaw due to roll control are two separate and distinct parameters, these quantities are tied together when considering vehicle control and handling qualities. Inherent static directional stability, if it exists, tends to counteract adverse yaw due to roll control. High angle-of-attack neutral static directional stability, however, in the presence of these adverse control effects, could lead to control and handling problems during entry.

Lifting body.- The longitudinal aerodynamic characteristics of the lifting body are presented in figures 15, 16, and 17 in relation to configuration buildup, elevon deflections, and tip-fin roll-out angles, respectively. The pitch data show that the vehicle was stable, trimmed, and very sensitive to elevon deflection (approximately 2.6° trim angle per degree of elevon deflection). Changing the tip-fin roll-out angle from 20° to 30° had little effect on the longitudinal aerodynamics (see fig. 17).

Directional and lateral stability characteristics are presented in figures 18, 19, and 20 as a function of configuration buildup, high and low trim angles, and tip-fin roll-out angles, respectively. The vehicle with $\theta = 30^\circ$ possessed lateral stability above $\alpha = 2^\circ$ and directional stability above $\alpha = 6^\circ$ with a negligible effect due to elevon deflection. A slight decrease in stability is observed for the $\theta = 20^\circ$ tip fin.

Entry-Maneuver—Aerothermodynamic Interactions

The entry trajectory parameters were calculated for a standard point mass with six degrees of freedom and a spherical nonrotating earth. Atmospheric cross range was achieved by constant-altitude trajectories with variations in the bank angle and angle of attack. The bank-angle variations consisted of a fixed angle from entry to pull-out, $\phi_e = 45^\circ$, modulation to maintain the constant altitude, a constant angle after the constant altitude hold, $\phi_f = 45^\circ$, and a zero angle once the final heading angle had been reached. Some typical altitude-velocity curves are shown in figure 21 for constant angle of attack and pitch-modulated entry modes. The bank-angle maneuvers are indicated for the constant angle-of-attack case.

The aerodynamic characteristics required for these entries were obtained over a Mach number range by extrapolating the experimental trim data for the wing-body configuration over an angle-of-attack range from 15° to 45° . The data were assumed to vary linearly with Mach number for each α from $M = 22$ to $M = 6$ (unpublished data), as shown in figure 22(a). The hypersonic aerodynamic predictions for this same vehicle neglecting viscous effects (presented in ref. 1) were used for the theoretical $M = 20$ aerodynamics, and they were also extrapolated to $M = 6$ in a similar manner (fig. 22(b)).

As suggested in reference 1, the pitch maneuver for the vehicle with a theoretical $(L/D)_{\max}$ of 2.4 at $M = 20$ was initiated at $M = 20$ and continued down to $M = 8$ (see fig. 23) in order to obtain a cross range of 1500 n. mi. Also shown for comparison is a constant angle-of-attack ($\alpha = 31^\circ$) entry which generates the same cross range. The maximum decelerations associated with these maneuvers for both modes were approximately 1.6g.

The stagnation heating rates and the lower-surface maximum-radiation equilibrium temperature (ref. 4) for the theoretical $(L/D)_{\max} = 2.4$ vehicle operating in the two

entry modes are shown in figures 24 and 25. Compared with the constant $\alpha = 31^\circ$ case, the pitch-modulated mode resulted in lower stagnation heating rates, lower total heat load, and equivalent soak times. Although the stagnation heating rates were lower for the pitch-modulated case, the maximum-radiation equilibrium temperatures over the lower surface were slightly higher. These temperatures were higher because the maximum-stagnation heating rate for the pitching mode occurred at a higher angle of attack (45°) with higher values of the ratio of local \dot{q} to stagnation \dot{q} and, consequently, higher local heating rates were obtained compared with the constant $\alpha = 31^\circ$ case. The entry angles γ_e indicated in figure 24 were chosen to equalize the pair of peak stagnation heating rates for each mode.

The stagnation heating-rate histories (ref. 4) are compared in figure 26 for a lower-performance ($(L/D)_{\max} = 2$ based on experimental data) vehicle operating at a constant angle of attack and with a pitch-modulated entry mode. For the fixed-attitude case, the angle of attack ($\alpha = 29.6^\circ$) was that required to generate 1500 n. mi. For one pitch-modulated case, the modulation from $\alpha = 45^\circ$ began at $M = 20$ as before but continued down to $\alpha = 15^\circ$ at $M = 16$ rather rapidly in order to obtain the desired cross range. The resulting rapid decrease in lift coefficient caused a steep plunge with corresponding increases in the maximum stagnation heating rate of more than 60 percent compared with the fixed-attitude mode (fig. 26(a)). The total heat load and the soak time, however, were still greater for the fixed-attitude case.

By initiating the pitch modulation earlier than at $M = 20$ during entry, the cross-range objective can be reached by modulating the pitch over a longer time period with a decrease in the maximum heating rate. An example of the reduction in \dot{q} is shown in figure 26(b) for a pitch modulation from 45° at $M = 24$ down to 15° at $M = 12$. Compared with the pitch modulation from $M = 20$ to $M = 16$ and the $\alpha = 29.6^\circ$ cases, the total heat load is less with about the same soak time. The entry maneuvers and Mach number variations associated with these entry modes are shown in figure 27 for comparison. The maximum decelerations for these maneuvers were the same as before, 1.6g.

The lowest values of the maximum-radiation equilibrium temperatures over the lower surface of the delta-wing-body orbiter with an $(L/D)_{\max} = 2$ at $M = 20$ are compared in figure 28 for the different entry modes. A nose radius of 0.53 meter (1.75 ft) and an emissivity of 0.8 were assumed for the full-scale vehicle. Although the maximum stagnation heating rate was much greater when pitching from $M = 20$ to $M = 16$, the peak occurred at a low angle of attack (20°) where the local heating rate was relatively low. As a result, differences in the maximum-radiation equilibrium temperatures over a major portion of the lower surface for the different modes were judged to be small and in agreement with the values for the higher-performance case.

CONCLUDING REMARKS

The static longitudinal, directional, and lateral stability and control characteristics of two classes of lifting entry vehicles – a delta lifting body and a delta-wing body – have been obtained at a Mach number of 20 in helium for operational Reynolds numbers. The angles of attack varied from -4° to 55° at sideslip angles of 0° and 4.5° . The aerodynamic characteristics of the wing-body orbiter were then evaluated in an entry-analysis study to examine the effects of vehicle performance on the aerothermodynamic parameters associated with constant and variable angle-of-attack modes for a 1500-n.-mi. cross range.

The wind-tunnel results showed that the vehicles can be trimmed with longitudinal static stability from an angle of attack near that for maximum lift-drag ratio to an angle of attack near that for maximum lift coefficient. In the operational angle-of-attack range, both vehicles had lateral stability, but the wing-body shape had neutral directional stability while the lifting body was directionally stable. Roll-control tests on the wing-body vehicle showed that it also had adverse yaw due to roll control. This roll-yaw coupling was not examined for the lifting body.

The entry trajectory analysis showed that a decrease in maximum vehicle performance from a maximum lift-drag ratio of 2.4 to 2.0 (on the order of 17 percent) required little change in the entry maneuvers for the constant angle-of-attack mode to achieve a nominal cross range of 1500 n. mi., but a change was required for the pitch-modulated mode. For the constant angle-of-attack entry, the decrease in performance resulted in no change in the maximum-stagnation heating rate, a decrease in total heat load, and a negligible change in soak time. For the pitch-modulated entry, the decrease in performance required the pitch initiation to begin early at a Mach number of 24 and to continue over a longer time period to a Mach number of 12 in order to meet the 1500-n.-mi. cross range without a major heating penalty. A comparison of the maximum laminar radiation equilibrium temperature on the lower surface showed that the reduction in performance had little effect regardless of the entry mode.

Langley Research Center,
National Aeronautics and Space Administration,
Hampton, Va., April 4, 1972.

APPENDIX

STING-EFFECT STUDY ON THE STATIC LONGITUDINAL AERODYNAMIC CHARACTERISTICS

Test Apparatus

All models were mounted on a sting-supported six-component strain-gage balance. Because of the limitation of the angle-of-attack mechanism ($\pm 18^\circ$), two sets of stings were required to cover the angle-of-attack range from -4° to 55° . A straight sting extending from the model bases was used for angles from -4° to 18° , while for $18^\circ \leq \alpha \leq 55^\circ$ the wing body was supported by a sting from the top of the model and the lifting body was supported by a dog-leg sting (figs. 29 and 30).

Longitudinal Aerodynamic Results

Delta-wing body. - A comparison of the longitudinal aerodynamic data for the two sting arrangements shown in figure 29 is presented in figure 31. The good agreement between the data for the two arrangements indicates there was negligible sting interference for the sting extending straight out of the base at the higher angles of attack.

Delta lifting body. - For the low angle-of-attack and the sideslip tests, the model was supported on a sting that extended straight back from the base (fig. 30(b)). For the high angle-of-attack tests at $\beta = 0^\circ$, the model was mounted on the dog-leg sting (fig. 30(a)) and on a straight sting for one check run.

A comparison of the longitudinal aerodynamic data using these different sting arrangements is presented in figure 32. Although the true hidden versus exposed sting comparison could not be made for this model, the results for the different sting arrangements indicate small differences.

REFERENCES

1. Anon.: Spacemaster – A Two-Stage Fully Reusable Space Transportation System, Phase A. MCR-69-36, Martin Marietta Corp., Dec. 1969.
2. Schramm, Wilson B.: Integral Launch and Reentry Vehicle. Vol. I – Configuration Definition and Planning, Pt. A. LMSC-A959837, Vol. I (Contract NAS 9-9206), Lockheed Missiles & Space Co., Dec. 22, 1969. (Available as NASA CR-102543.)
3. Anon.: Study of Integral Launch and Reentry Vehicle System. Vol. III. Technical Report – Second Phase Environment and Performance. SD 69-573-3 (Contract NAS 9-9205), North American Rockwell, Dec. 1969. (Available as NASA CR-102103.)
4. Arrington, James P.: Entry Maneuver/Aerothermodynamic Interactions for High Cross-Range Candidate Orbiters. Space Transportation System Technology Symposium, I – Aerothermodynamics and Configurations, NASA TM X-52876, Vol. I, 1970, pp. 509-530.
5. Arrington, James P.; Joiner, Roy C., Jr.; and Henderson, Arthur, Jr.: Longitudinal Characteristics of Several Configurations at Hypersonic Mach Numbers in Conical and Contoured Nozzles. NASA TN D-2489, 1964.

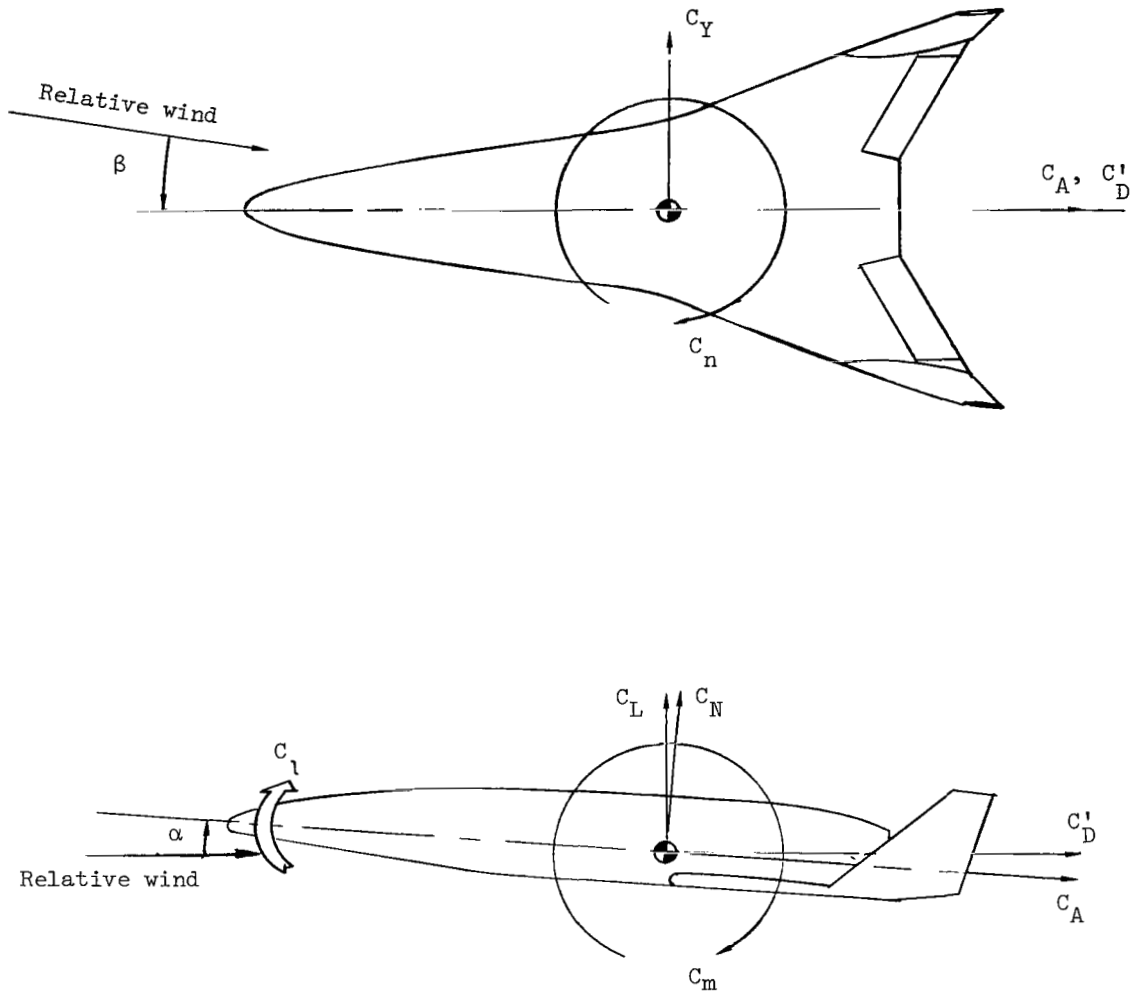
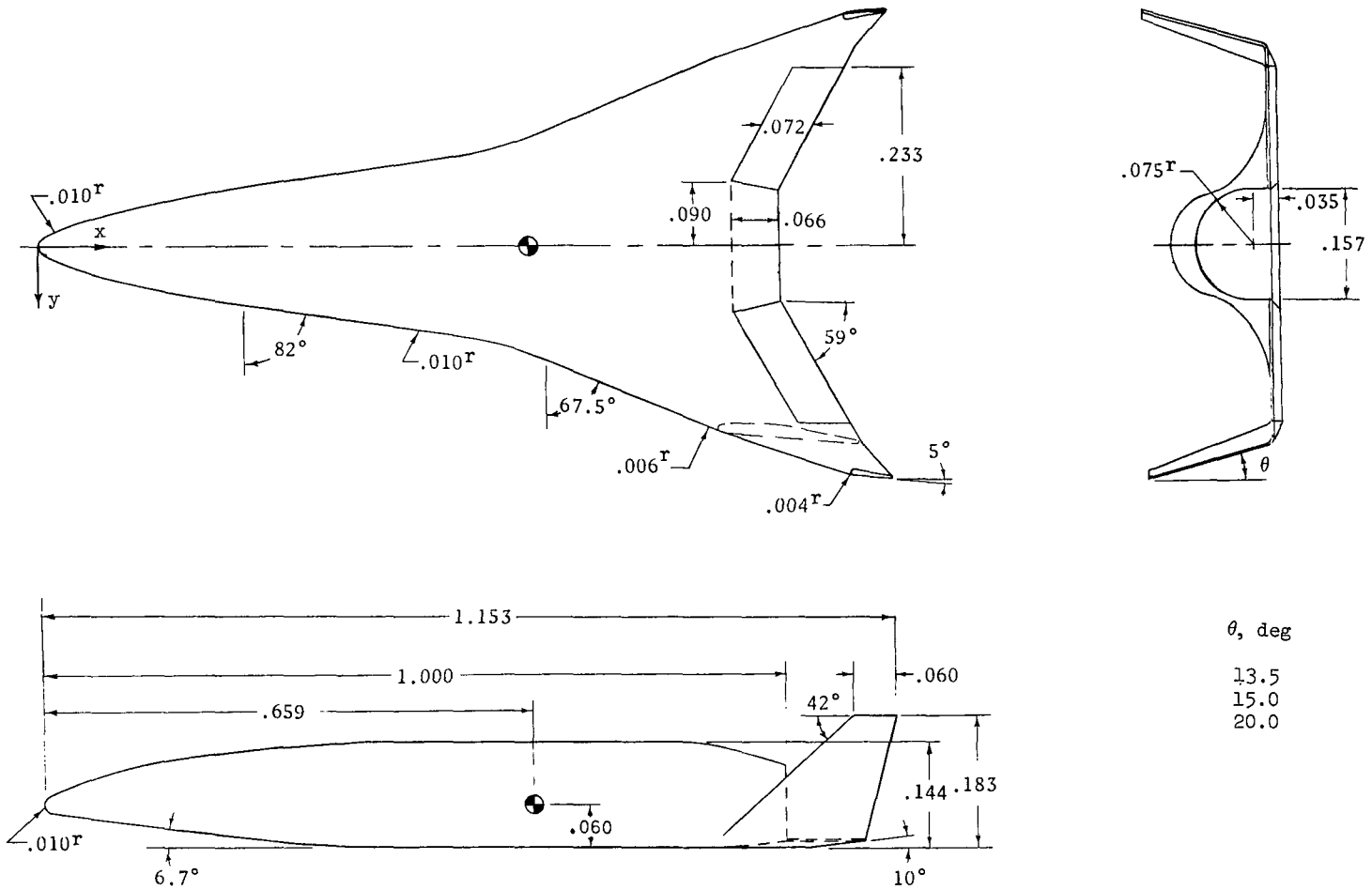


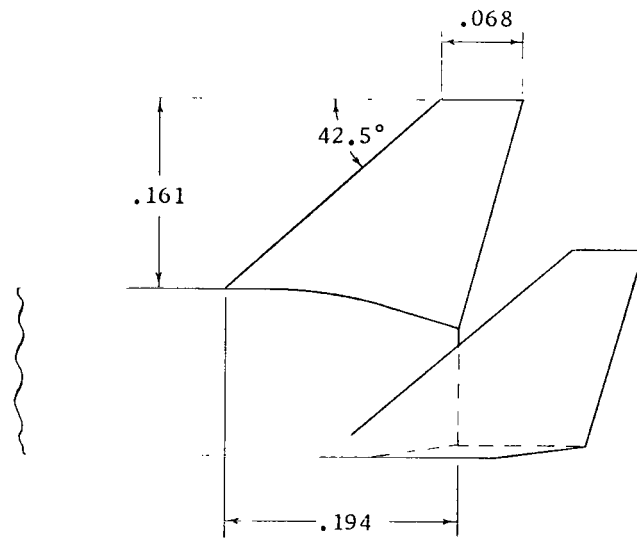
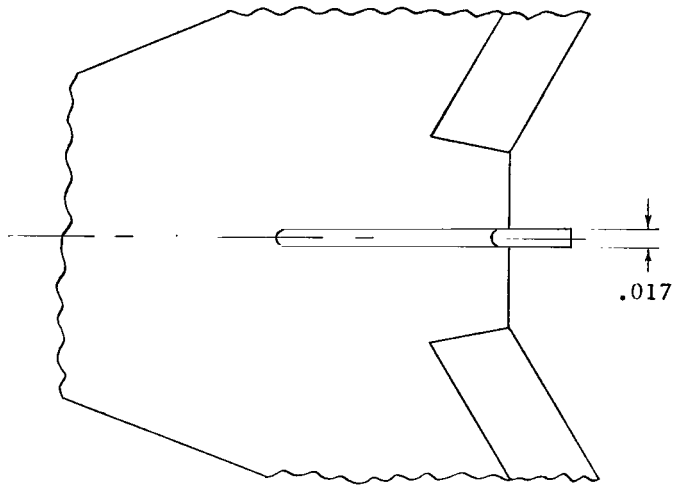
Figure 1.- Force and moment coefficients in the body and stability axis systems.
 (Arrows indicate positive directions of coefficients and angles.)



θ , deg
13.5
15.0
20.0

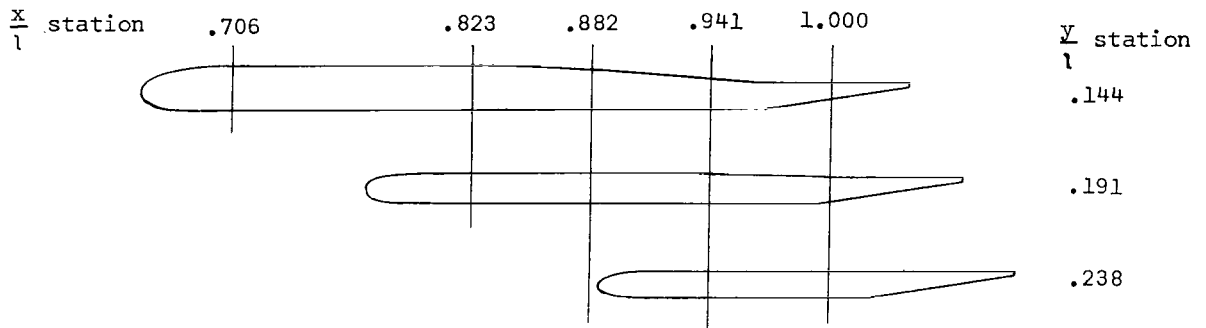
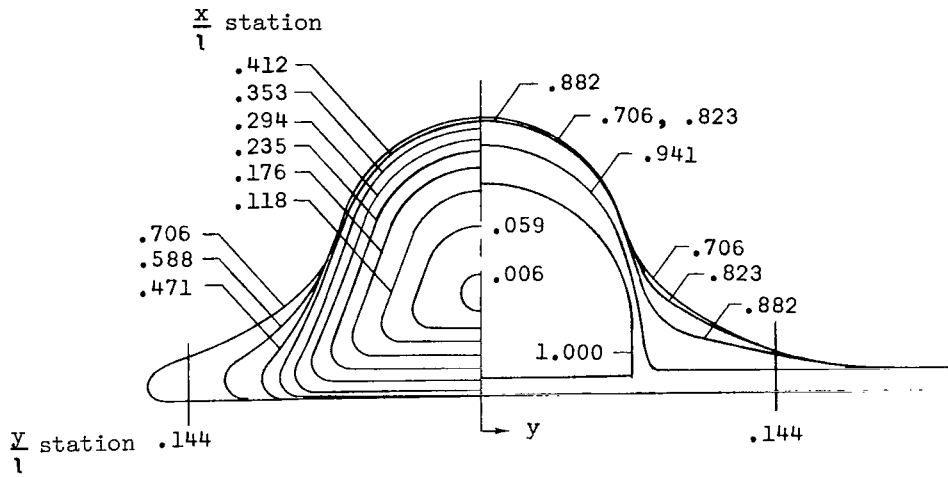
(a) With wing-tip fins.

Figure 2.- Wing-body configuration. (All dimensions are normalized in terms of body length, $l = 0.186 \text{ m} = 7.32 \text{ in.}$)



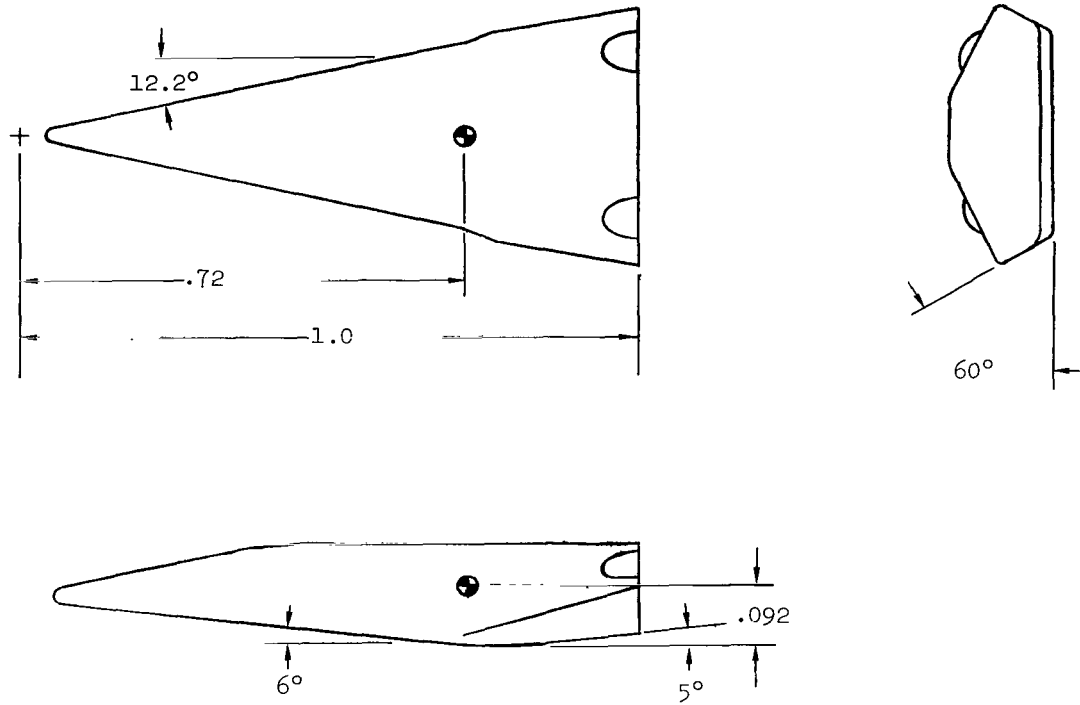
(b) With a body fin.

Figure 2.- Continued.



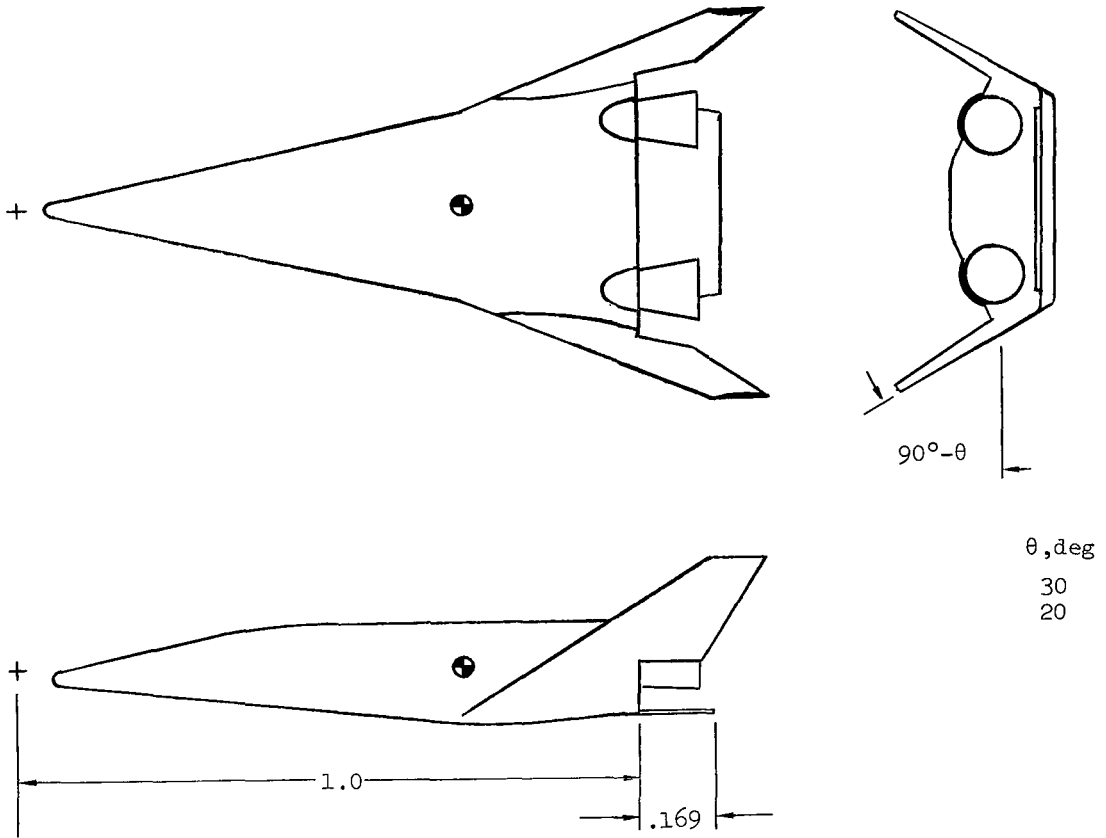
(c) Body and wing cross sections.

Figure 2.- Concluded.



(a) Body alone.

Figure 3.- Lifting-body configuration. (All dimensions are given in terms of reference length, $l = 0.150 \text{ m} = 5.9 \text{ in.}$)



(b) Complete configuration.

Figure 3.- Concluded.

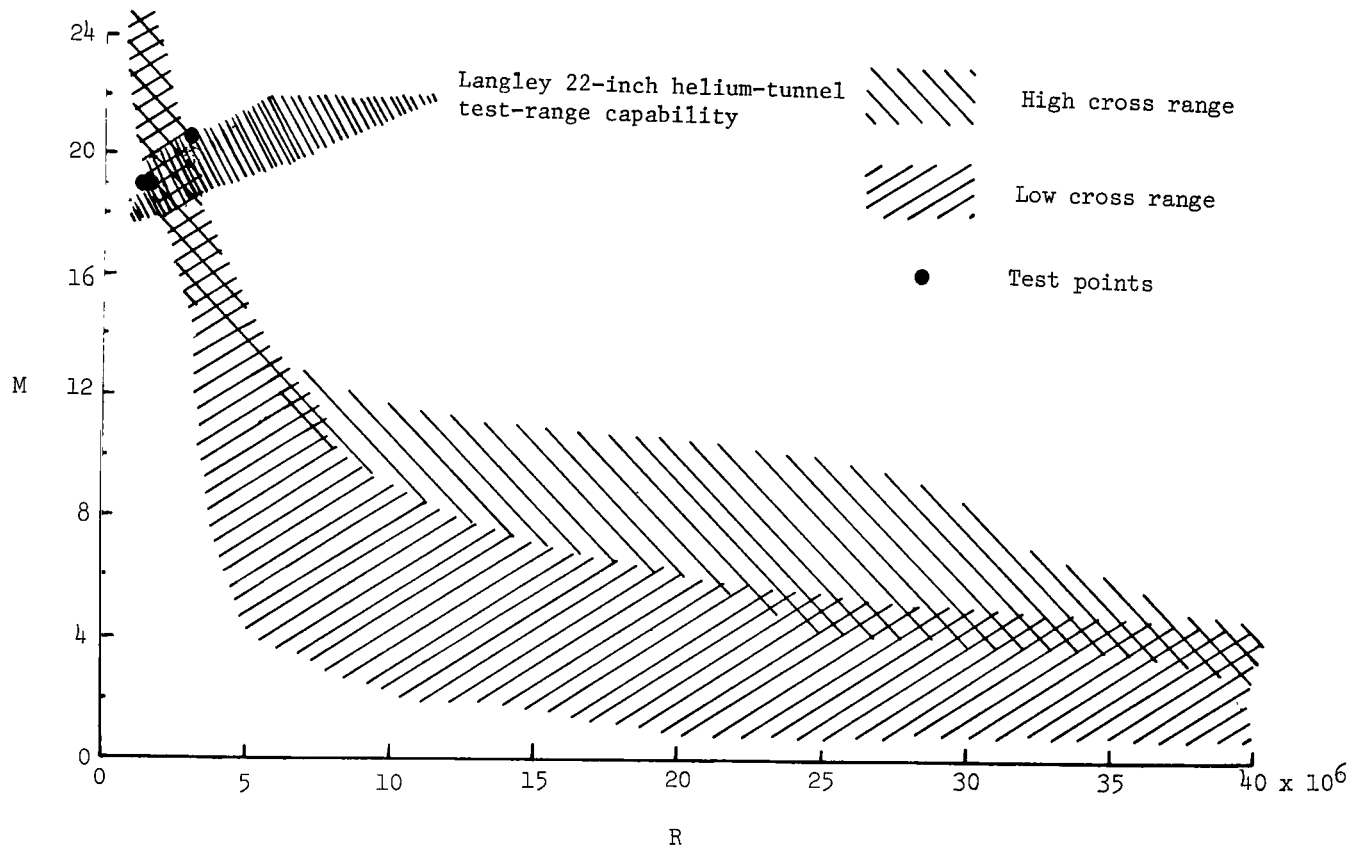


Figure 4.- Mach number—Reynolds number range for candidate (ILRV) shuttle orbiters during entry.

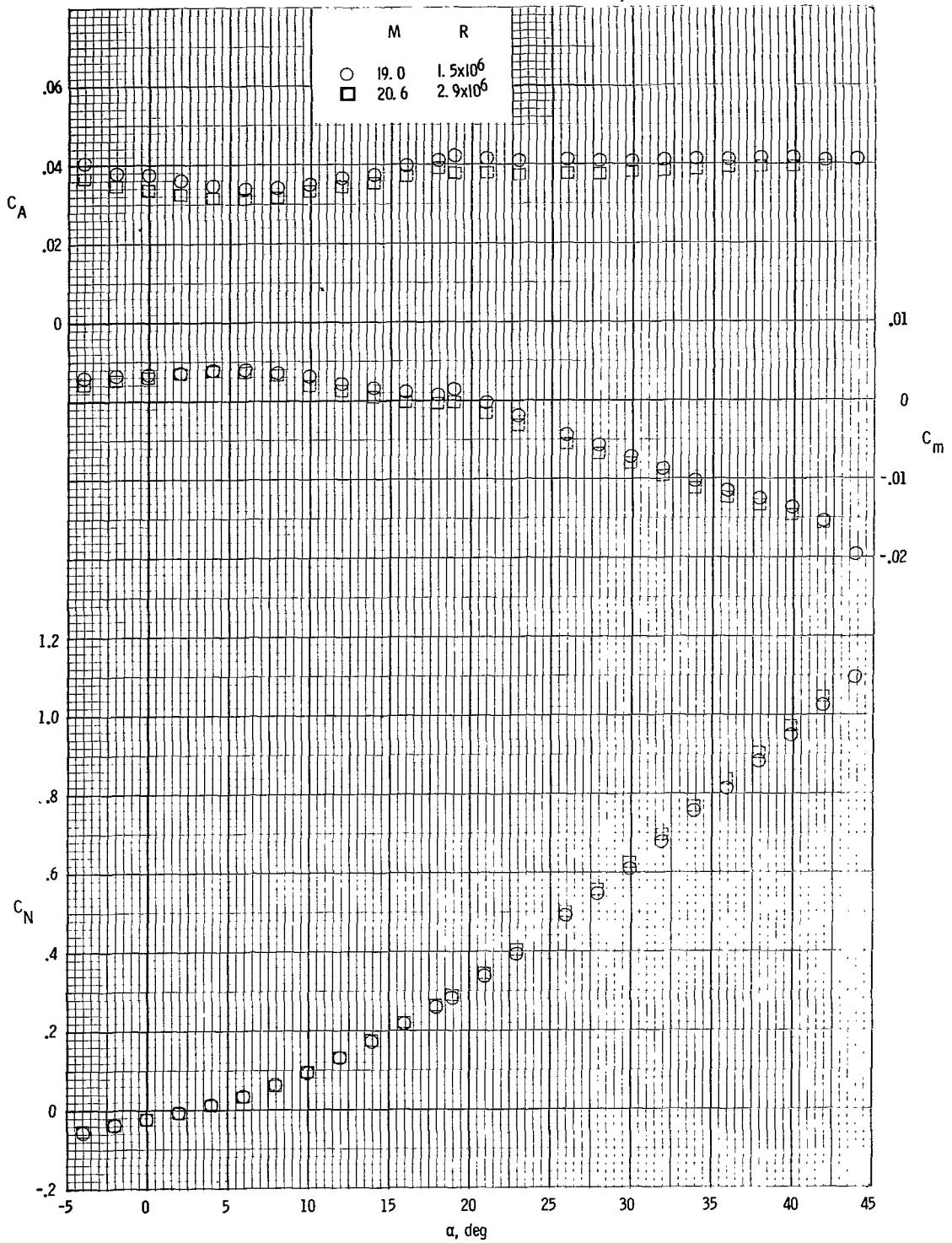


Figure 5.- Reynolds number effects on the aerodynamic characteristics of the wing-body configuration with $\delta_e = 20^\circ$ and $\theta = 13.5^\circ$.

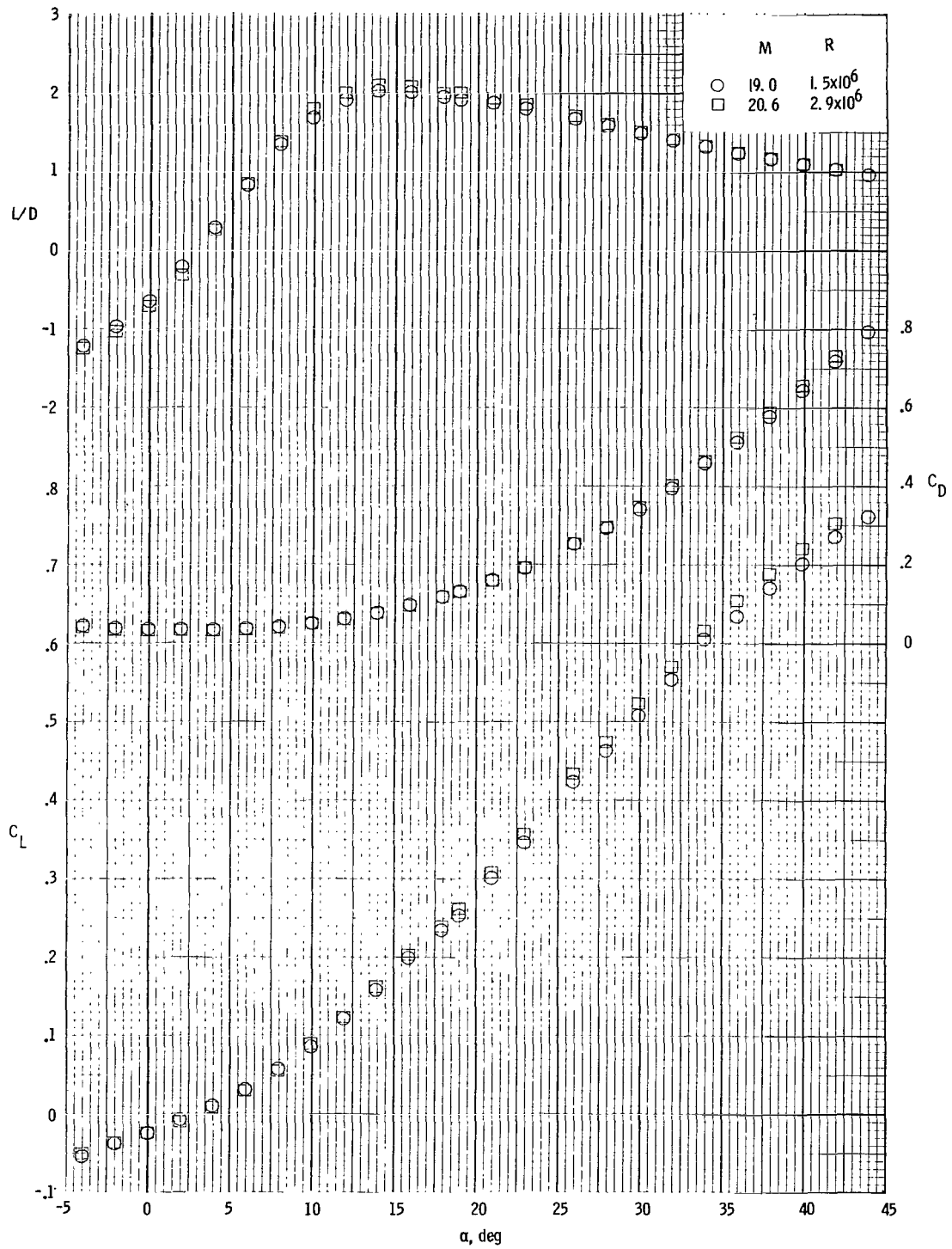


Figure 5.- Concluded.

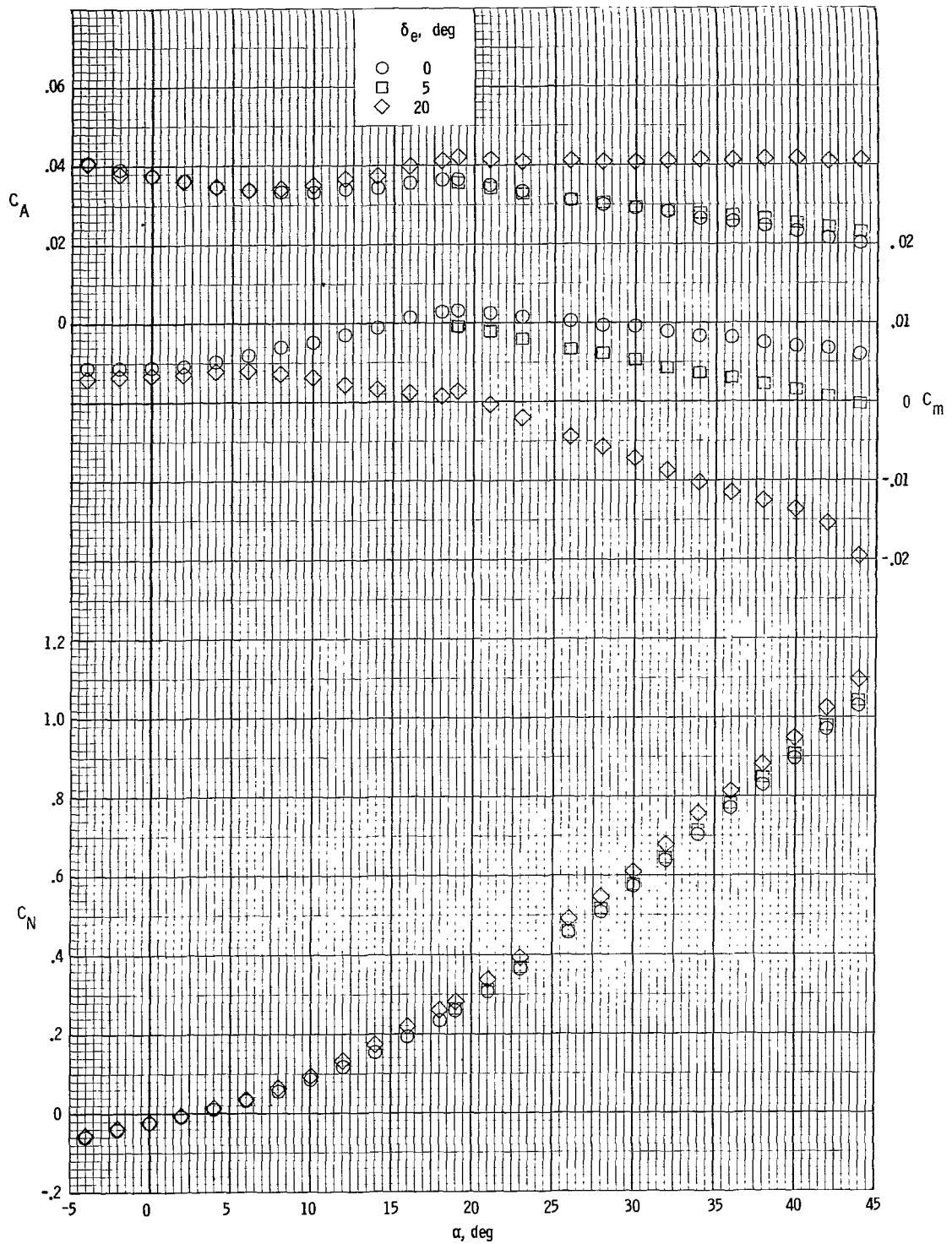


Figure 6.- Effect of elevon deflections on the longitudinal aerodynamic characteristics of the wing-body configuration with $\theta = 13.5^\circ$ at $M = 19$ and $R = 1.5 \times 10^6$.

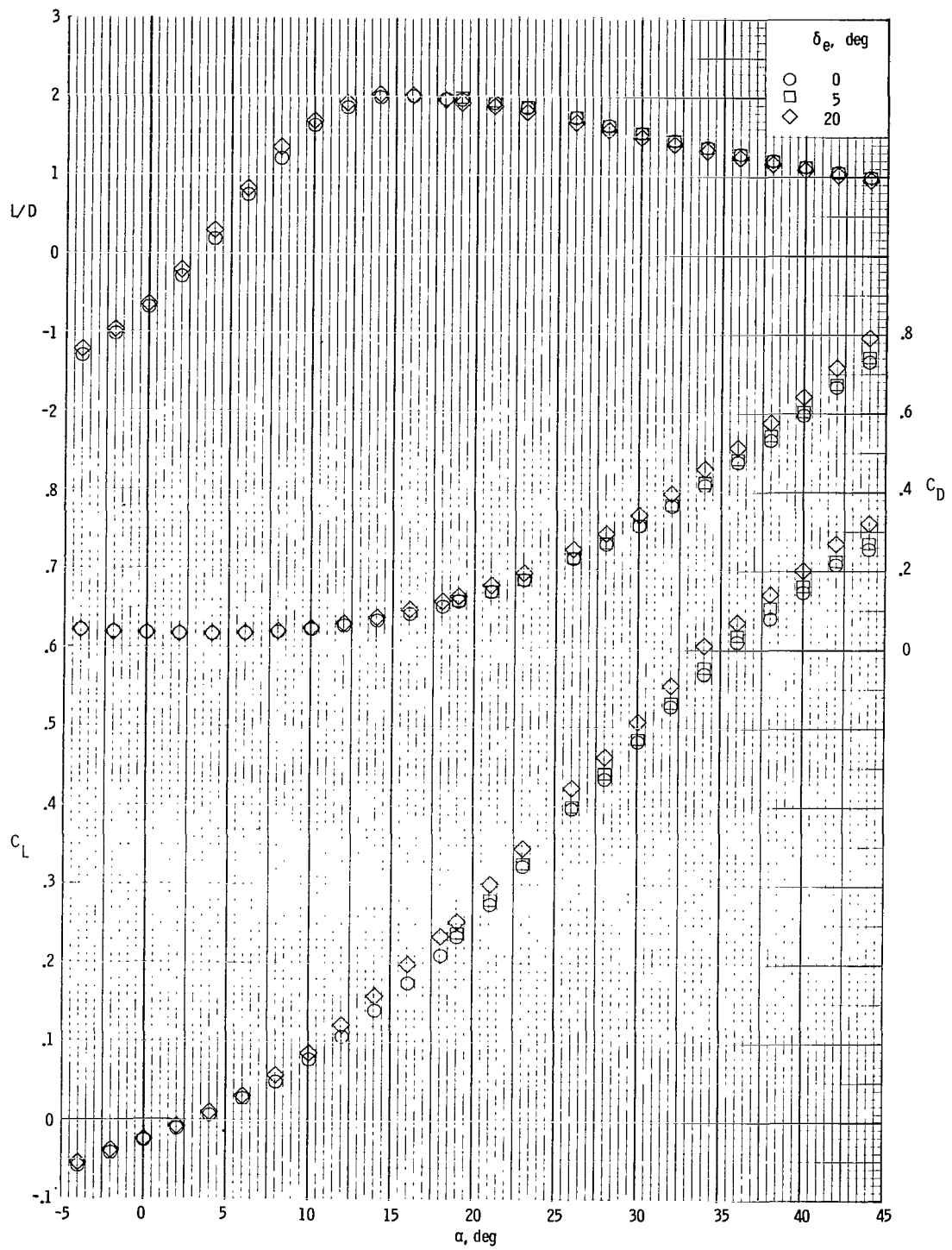


Figure 6.- Concluded.

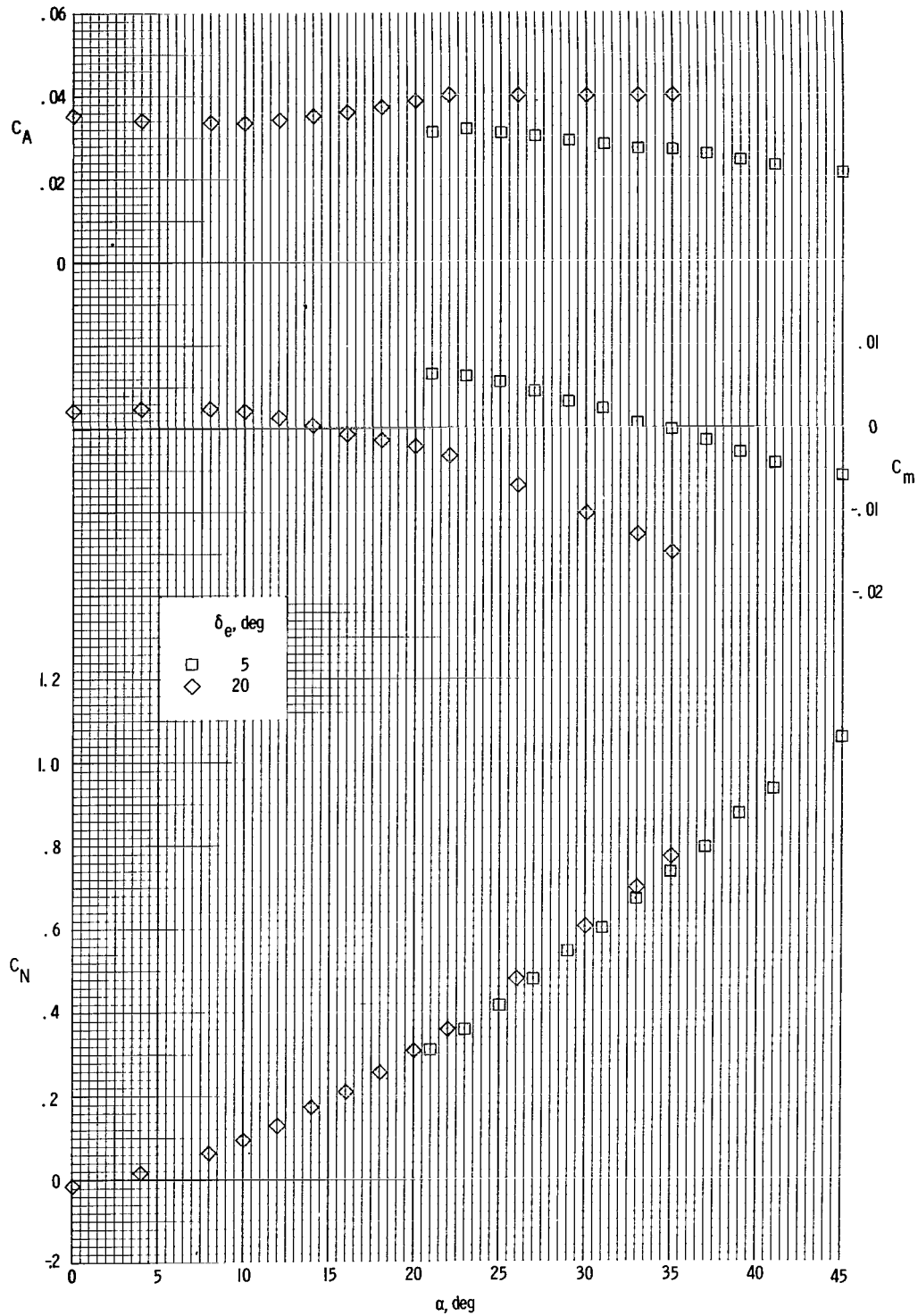


Figure 7.- Effect of elevon deflections on the longitudinal aerodynamic characteristics of the wing-body configuration with $\theta = 15^\circ$ at $M = 19$ and $R = 1.5 \times 10^6$.

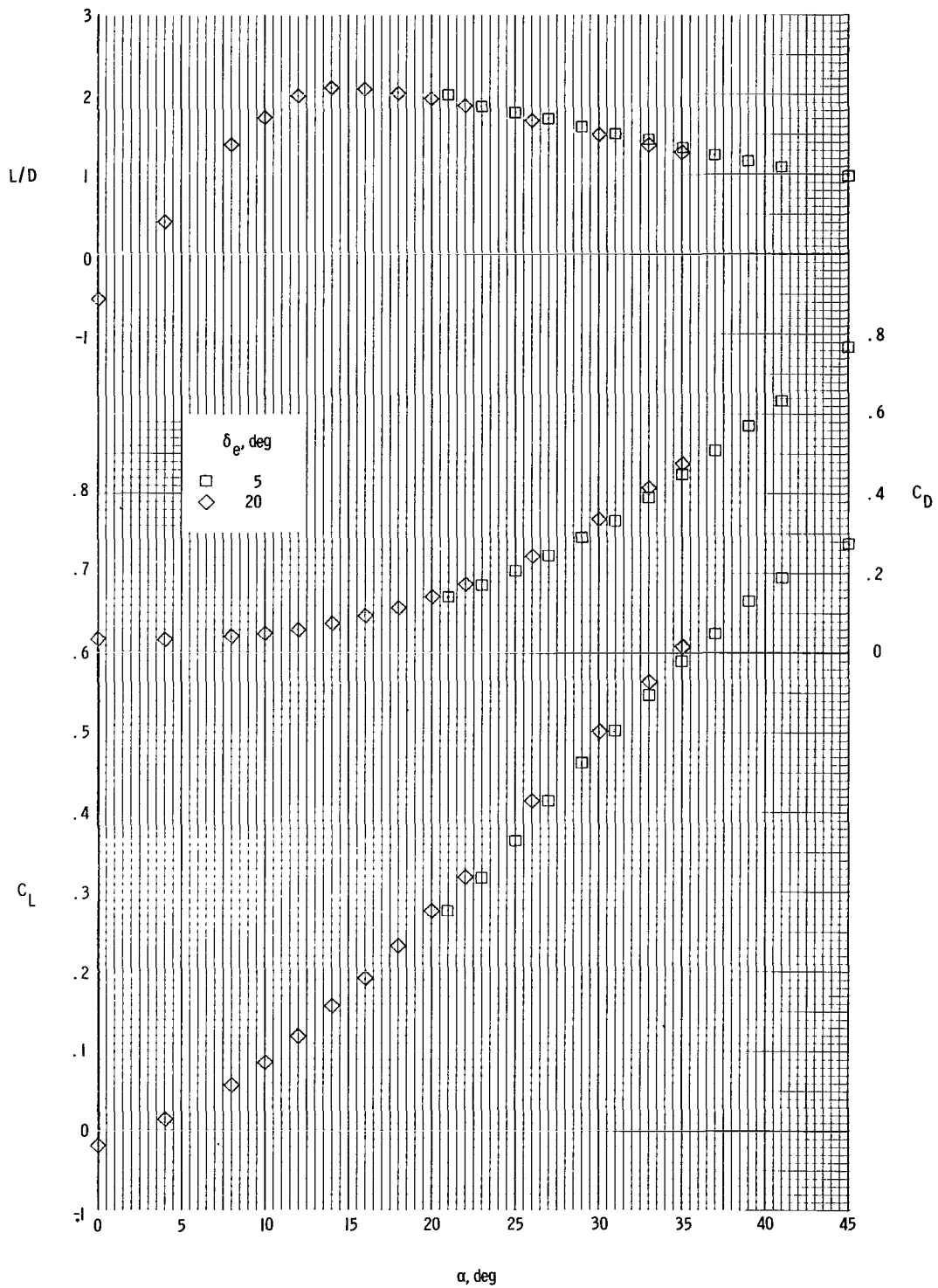


Figure 7.- Concluded.

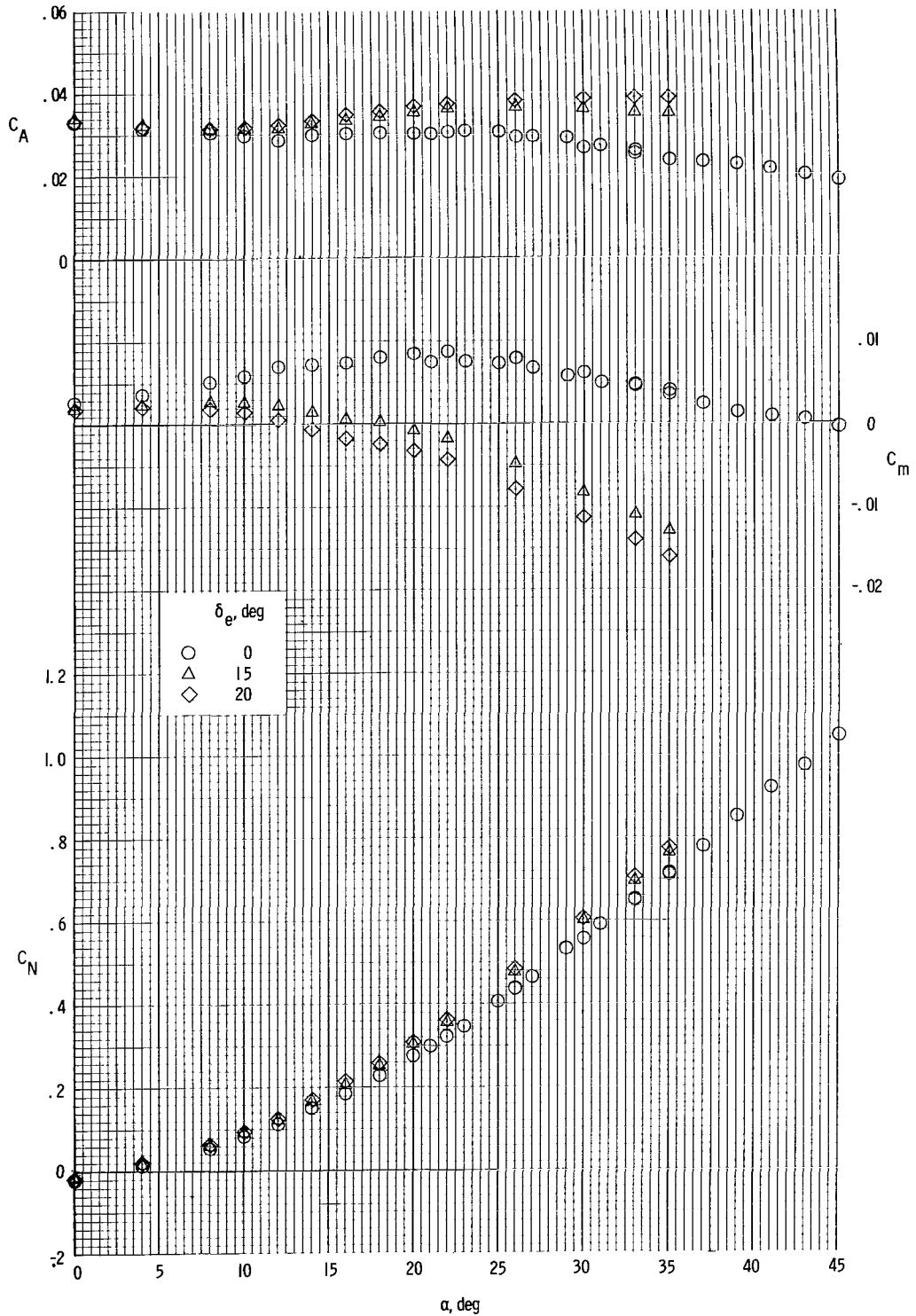


Figure 8.- Effect of elevon deflections on the longitudinal aerodynamic characteristics of the wing-body configuration with $\theta = 20^\circ$ at $M = 19$ and $R = 1.5 \times 10^6$.

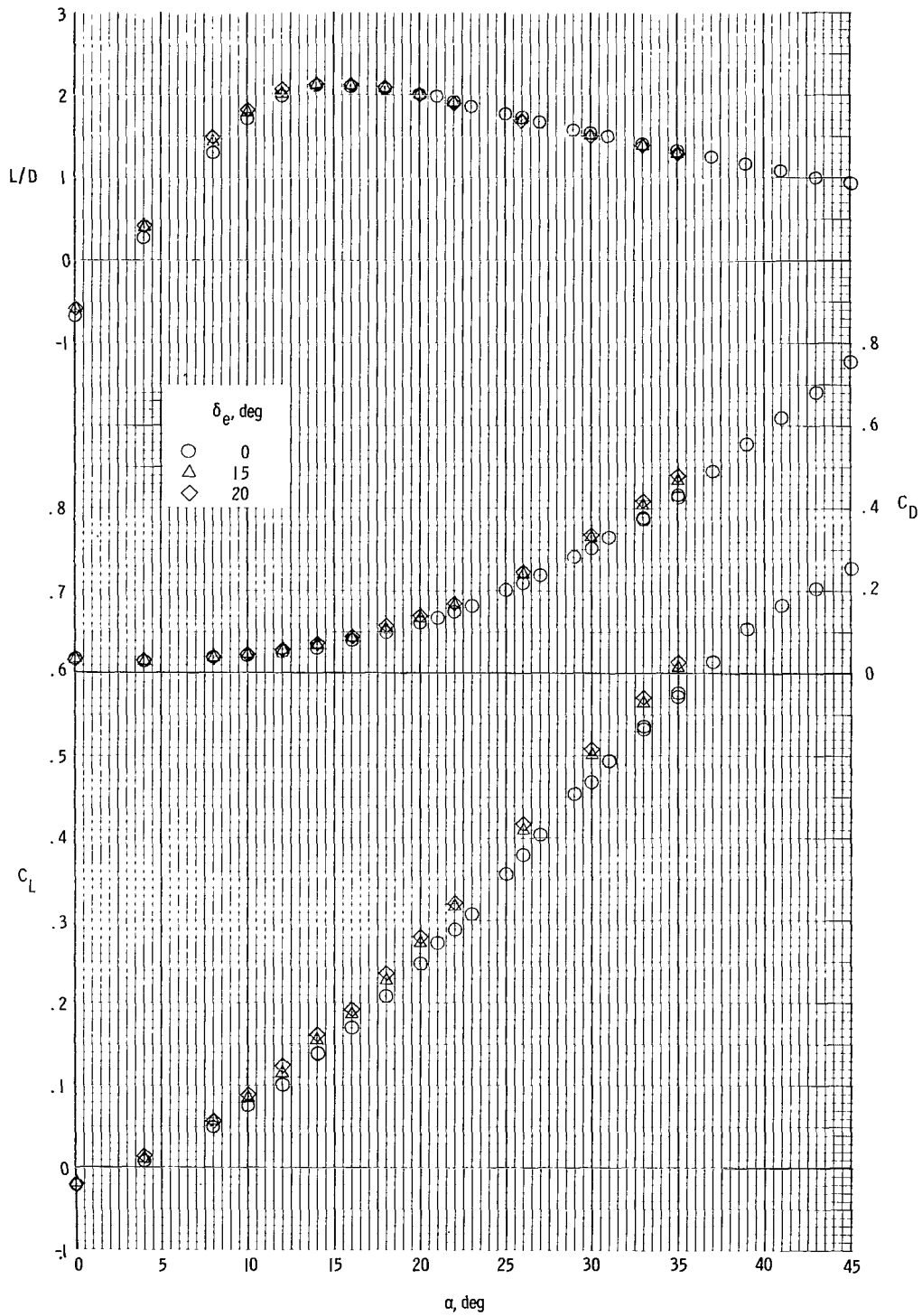


Figure 8.- Concluded.

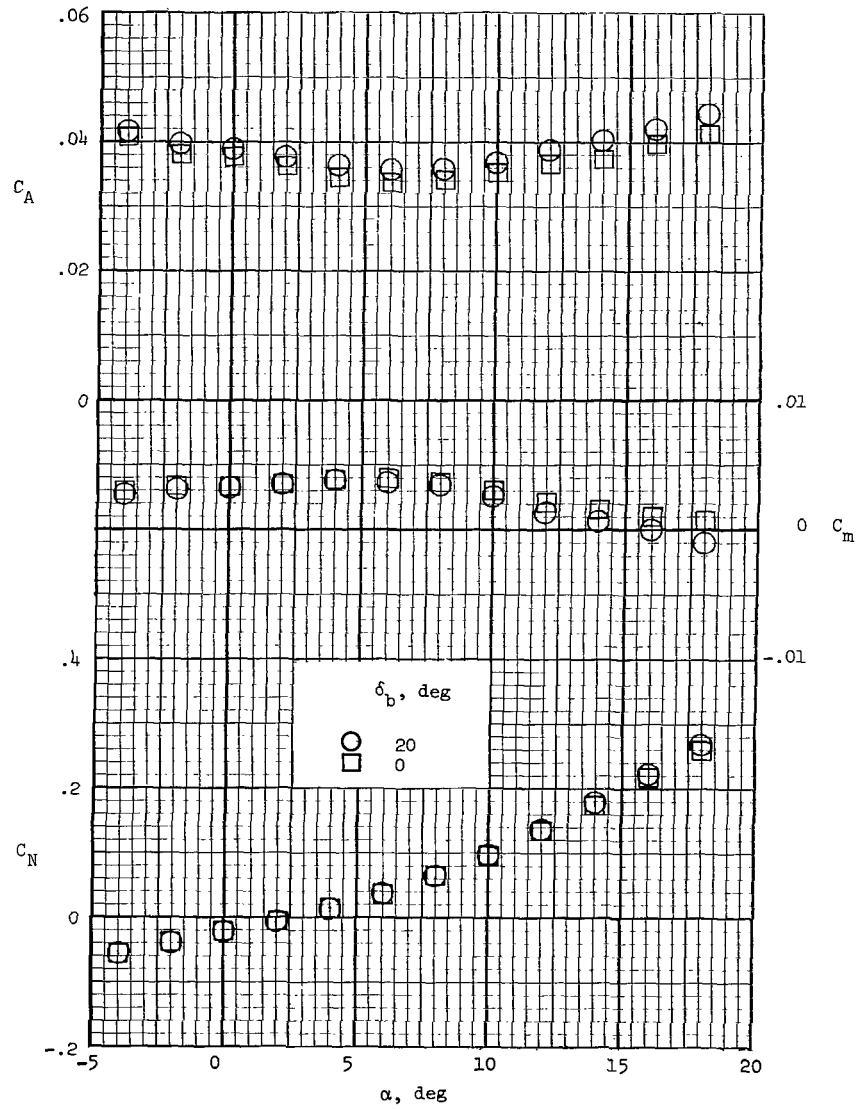


Figure 9.- Effect of body-flap deflection on the longitudinal aerodynamic characteristics of the wing-body configuration for $\delta_e = 20^\circ$ and $\theta = 13.5^\circ$ at $M = 19$ and $R = 1.5 \times 10^6$.

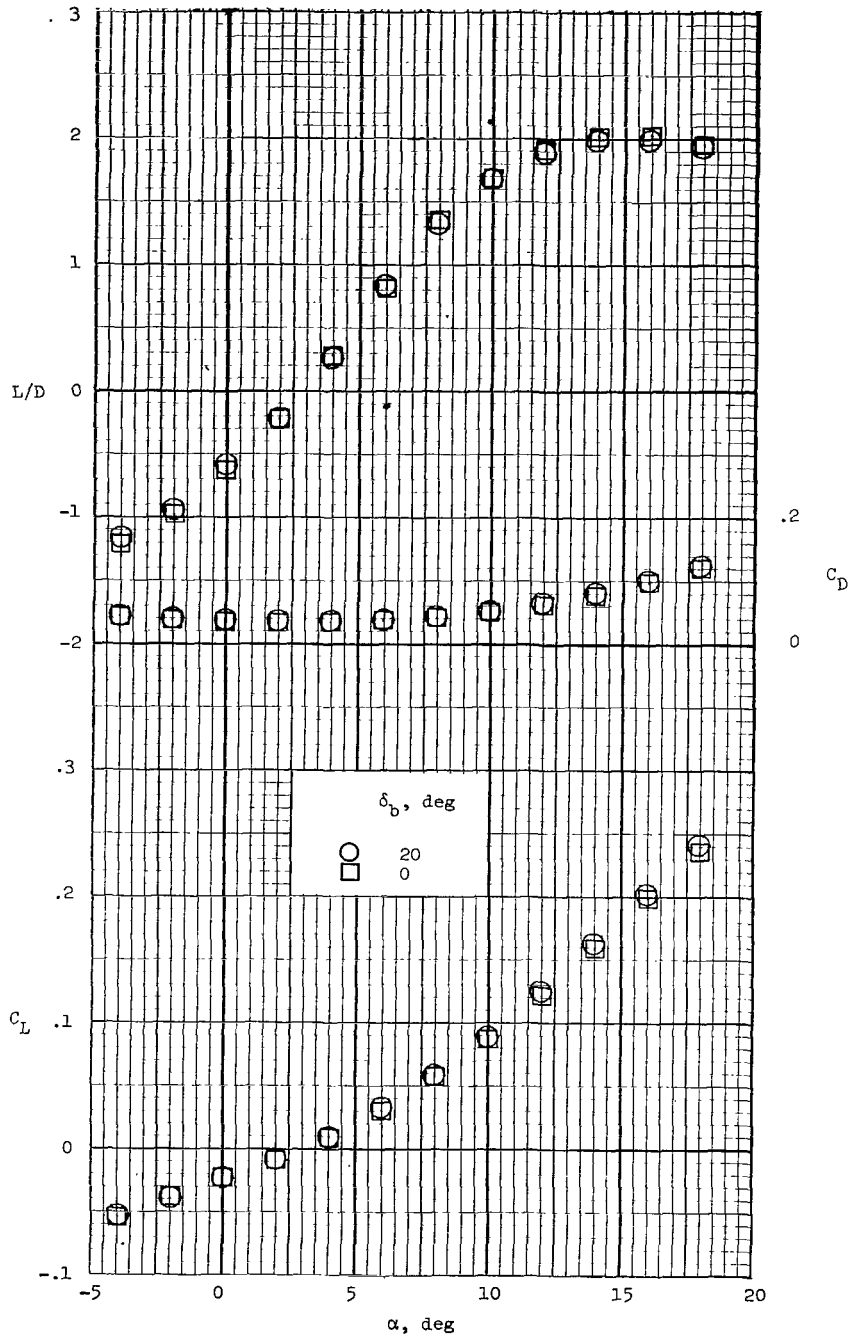


Figure 9.- Concluded.

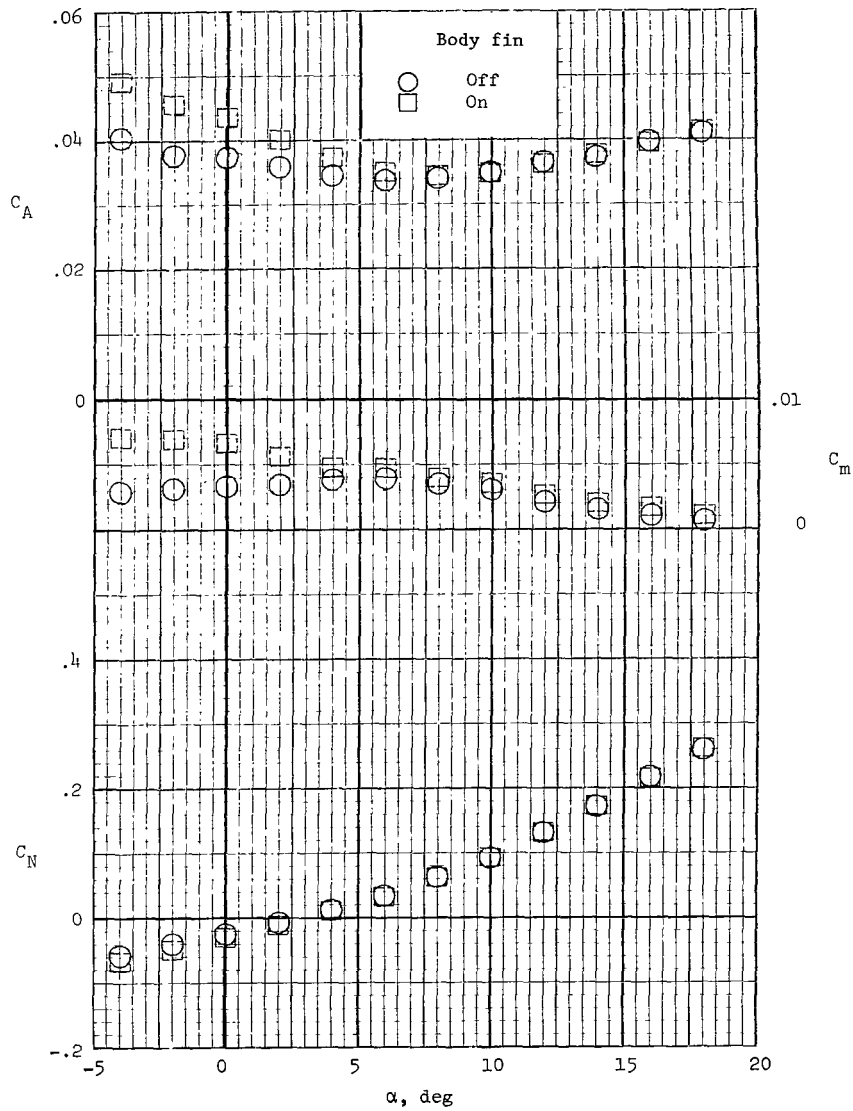


Figure 10.- Aerodynamic characteristics of the wing-body configuration with a body fin and $\theta = 13.5^\circ$ at $M = 19$ and $R = 1.5 \times 10^6$.

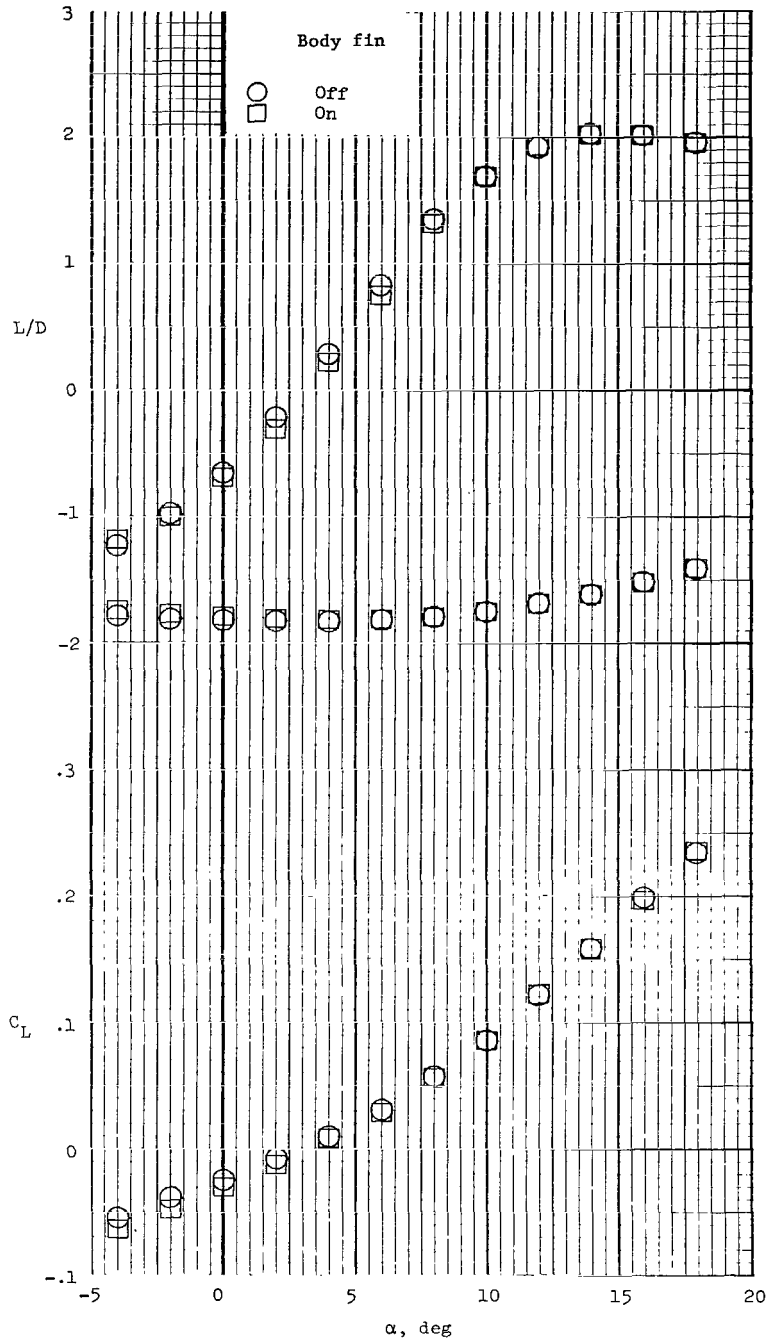


Figure 10.- Concluded.

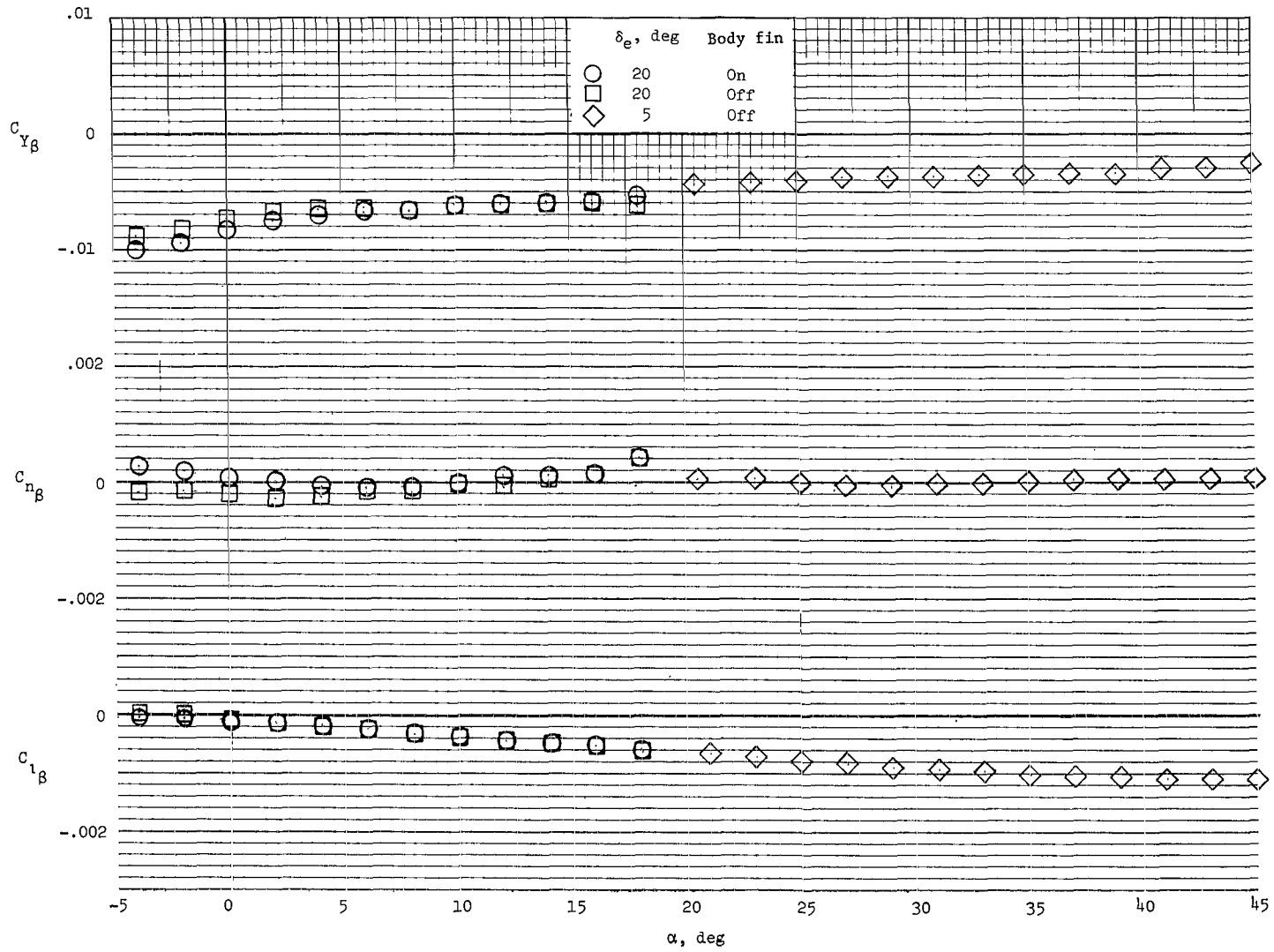


Figure 11.- Lateral and directional static stability characteristics of the wing-body configuration with $\theta = 13.5^\circ$ at $M = 19$ and $R = 1.5 \times 10^6$.

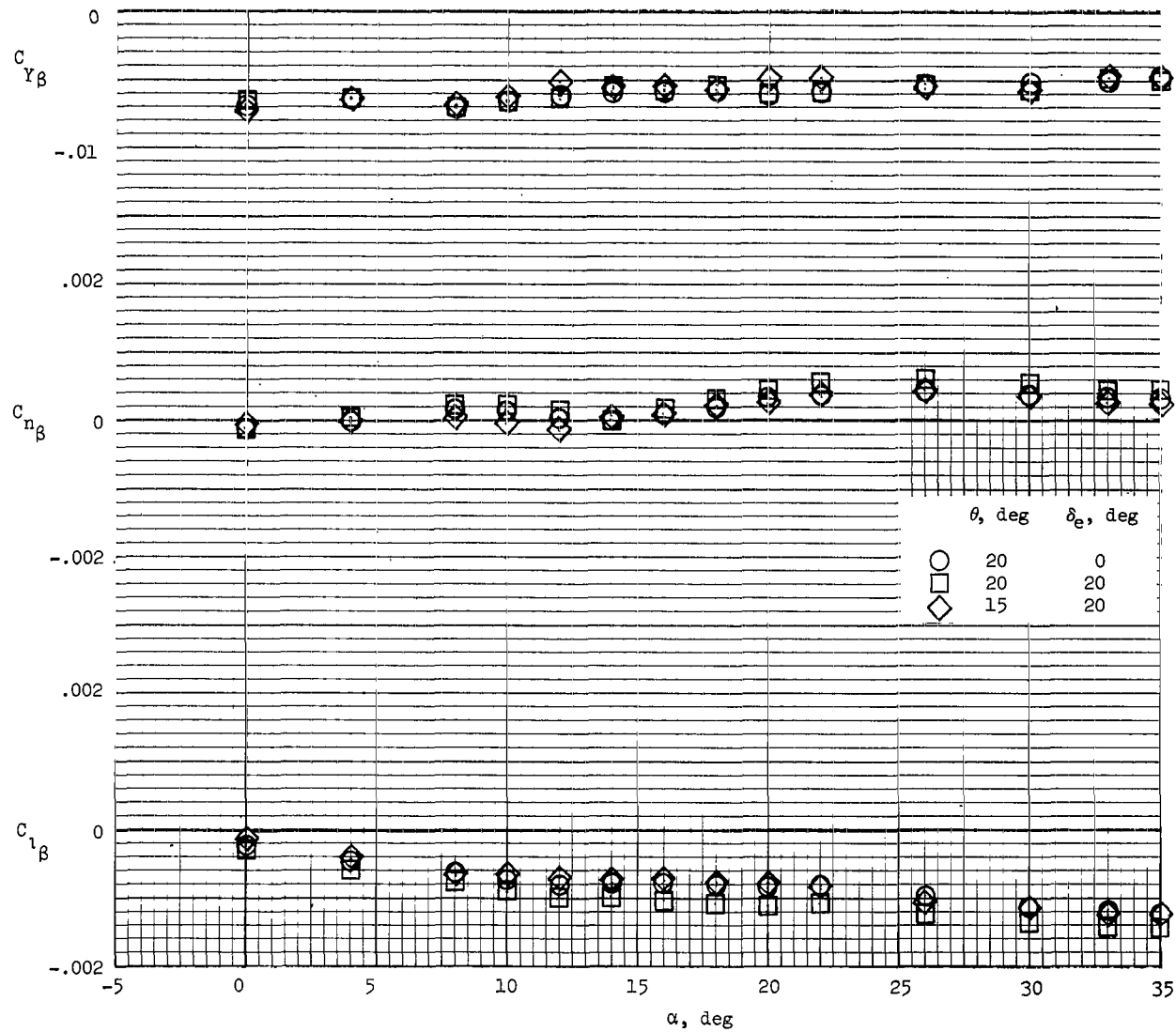


Figure 12.- Lateral and directional static stability characteristics of the wing-body configuration with two tip-fin roll-out angles at $M = 19$ and $R = 1.5 \times 10^6$.

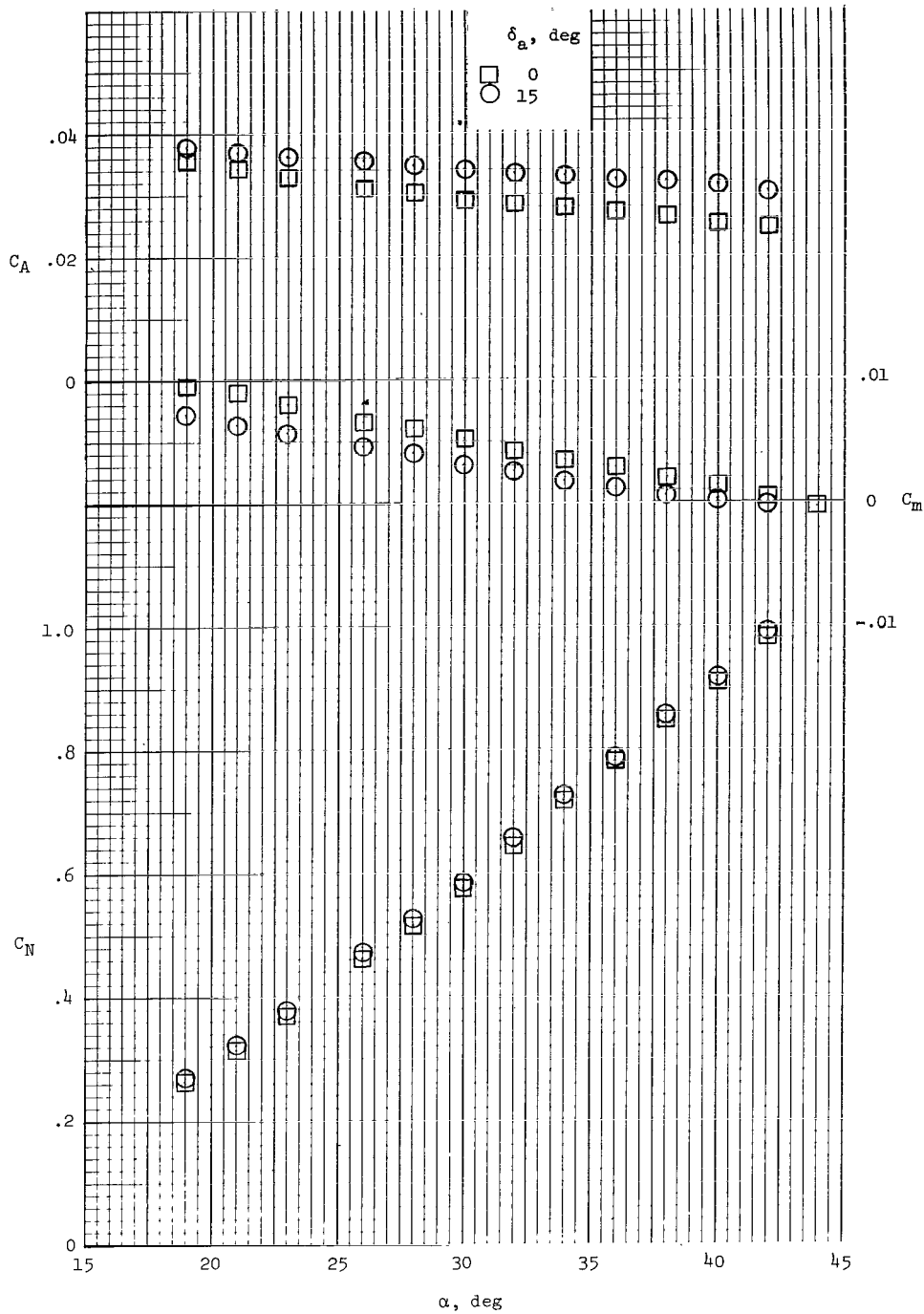


Figure 13.- Effect of aileron deflection on the aerodynamic characteristics of the wing-body configuration for $\delta_e = 5^\circ$ and $\theta = 13.5^\circ$ at $M = 19$ and $R = 1.5 \times 10^6$.

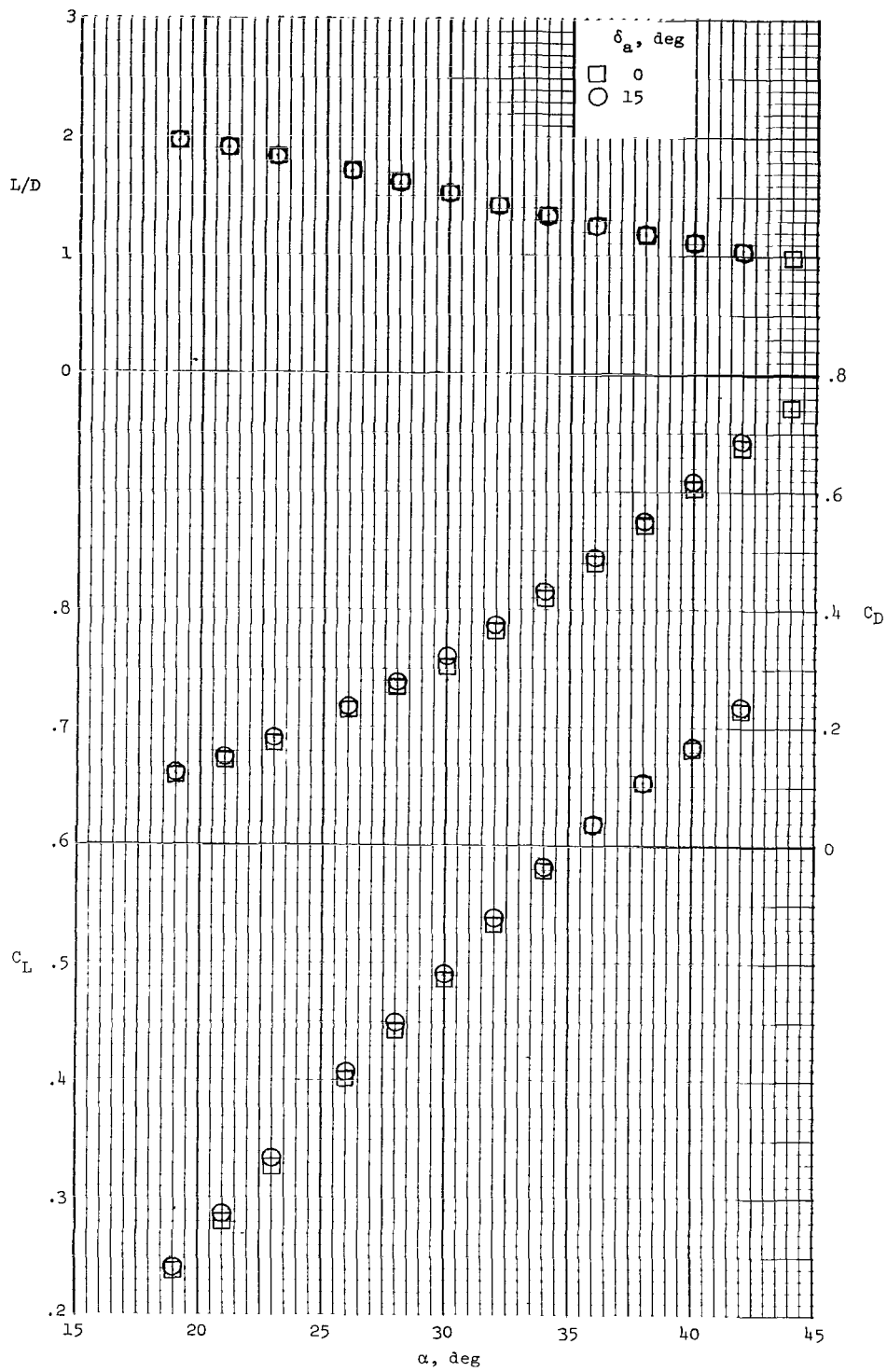


Figure 13.- Concluded.

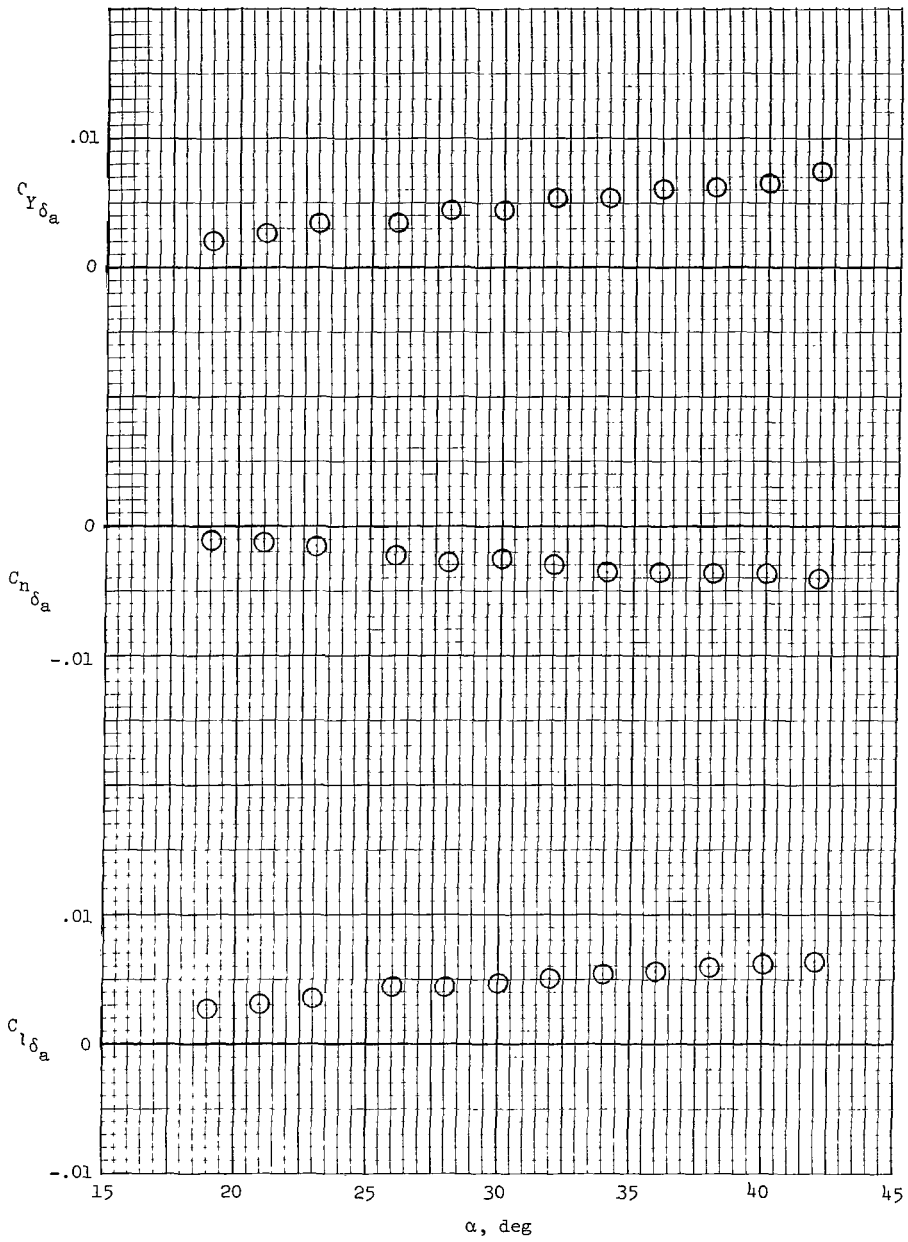


Figure 14.- Rate of change in lateral-directional characteristics of the wing-body configuration due to aileron deflection ($\delta_a = 15^\circ$) for $M = 19$ and $R = 1.5 \times 10^6$.

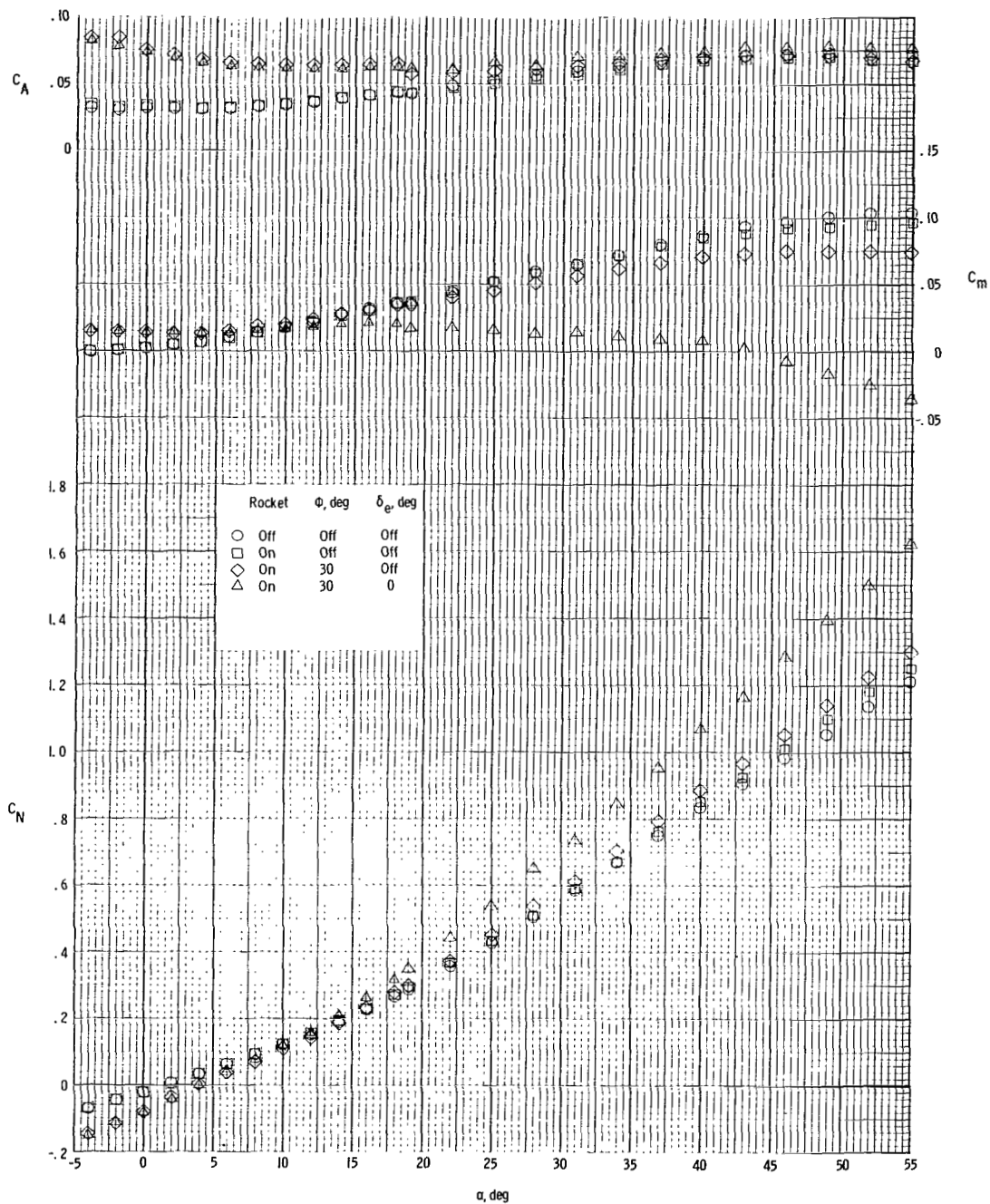


Figure 15.- Effect of configuration components on the longitudinal aerodynamic characteristics of the lifting-body configuration at $M = 19$ and $R = 1.28 \times 10^6$.

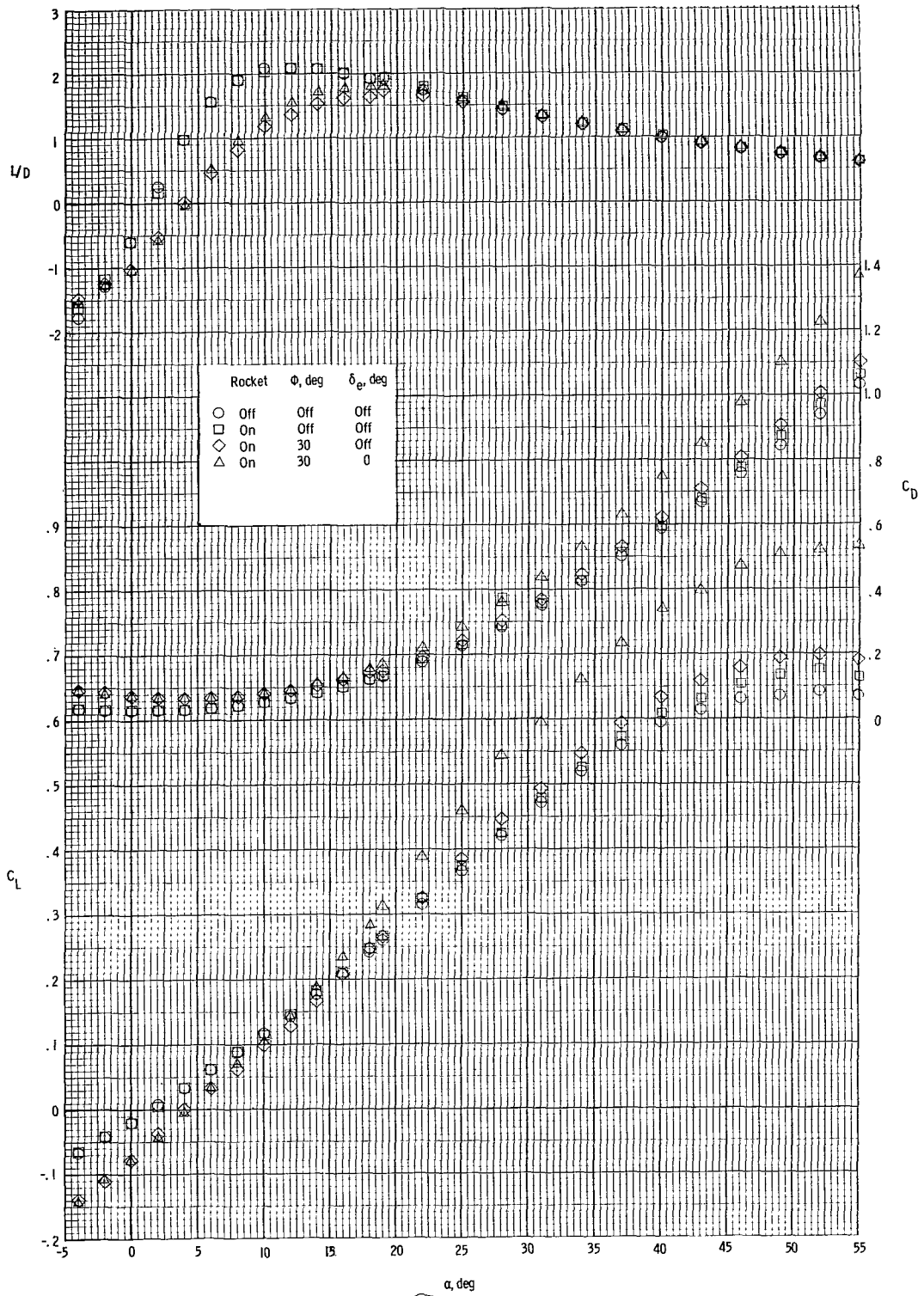


Figure 15.- Concluded.

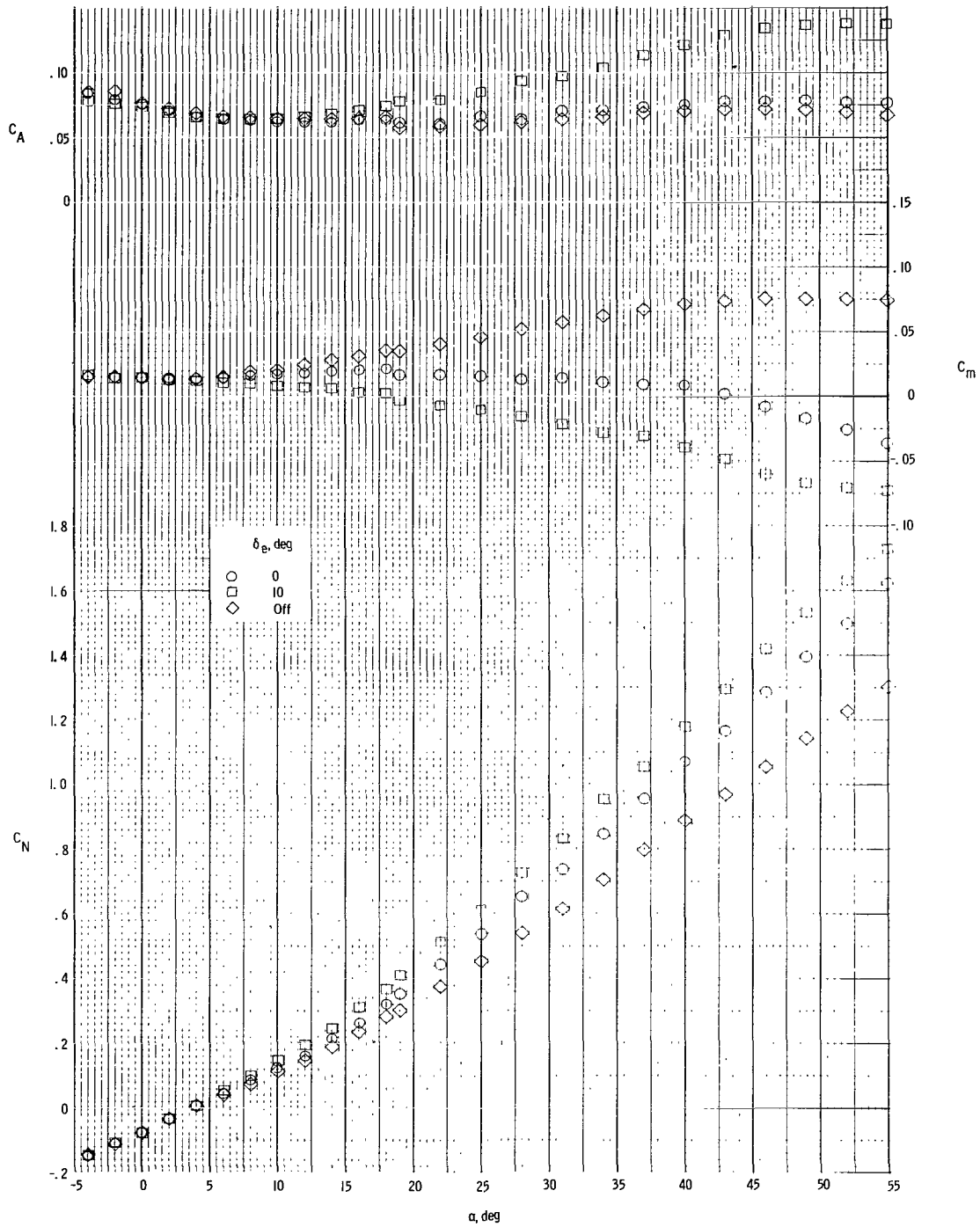


Figure 16.- Effect of longitudinal control on the longitudinal aerodynamic characteristics of the lifting-body configuration with $\theta = 30^\circ$ at $M = 19$ and $R = 1.28 \times 10^6$.

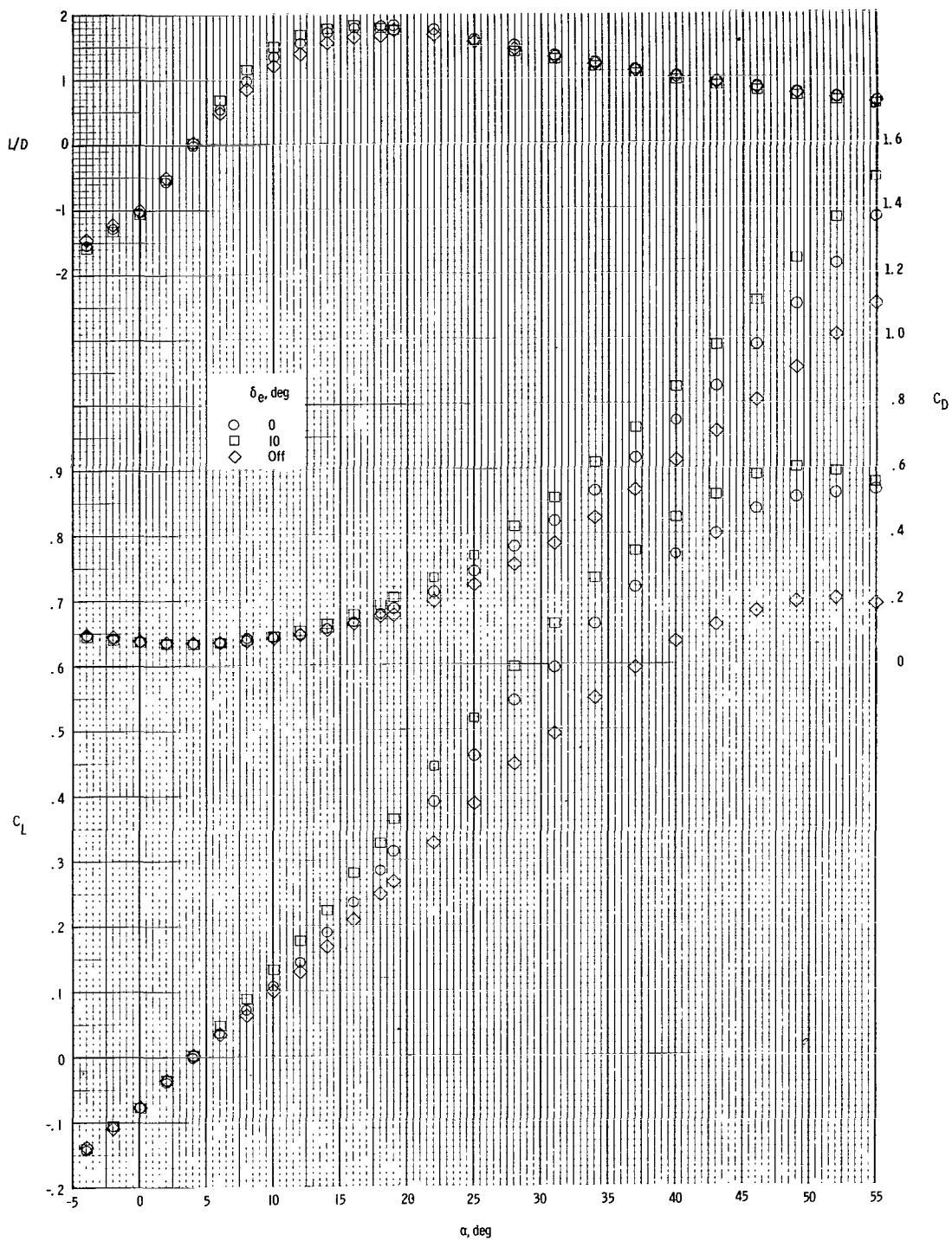


Figure 16.- Concluded.

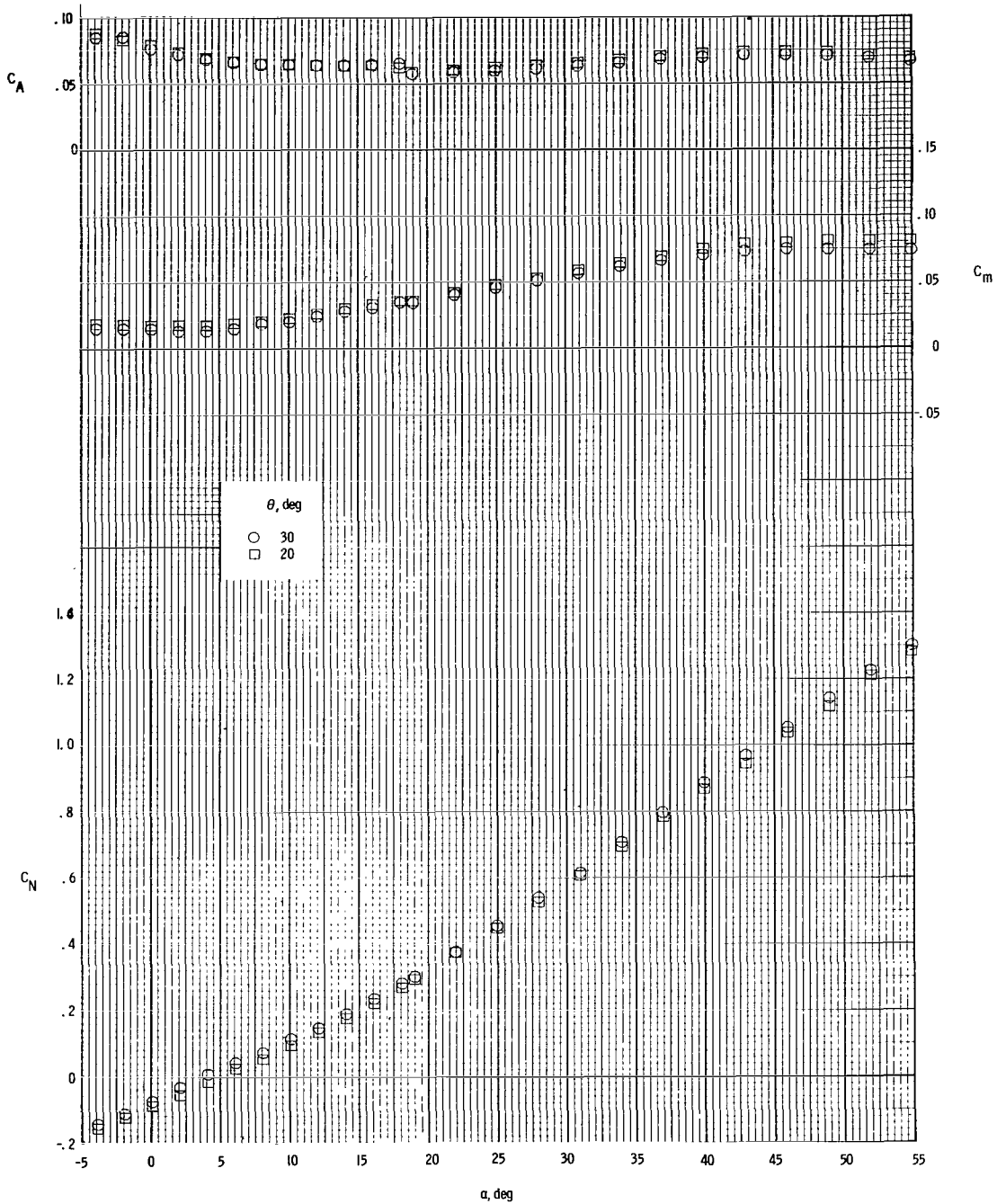


Figure 17.- Effect of tip-fin roll-out on the longitudinal characteristics of the lifting-body configuration with the elevons removed at $M = 19$ and $R = 1.28 \times 10^6$.

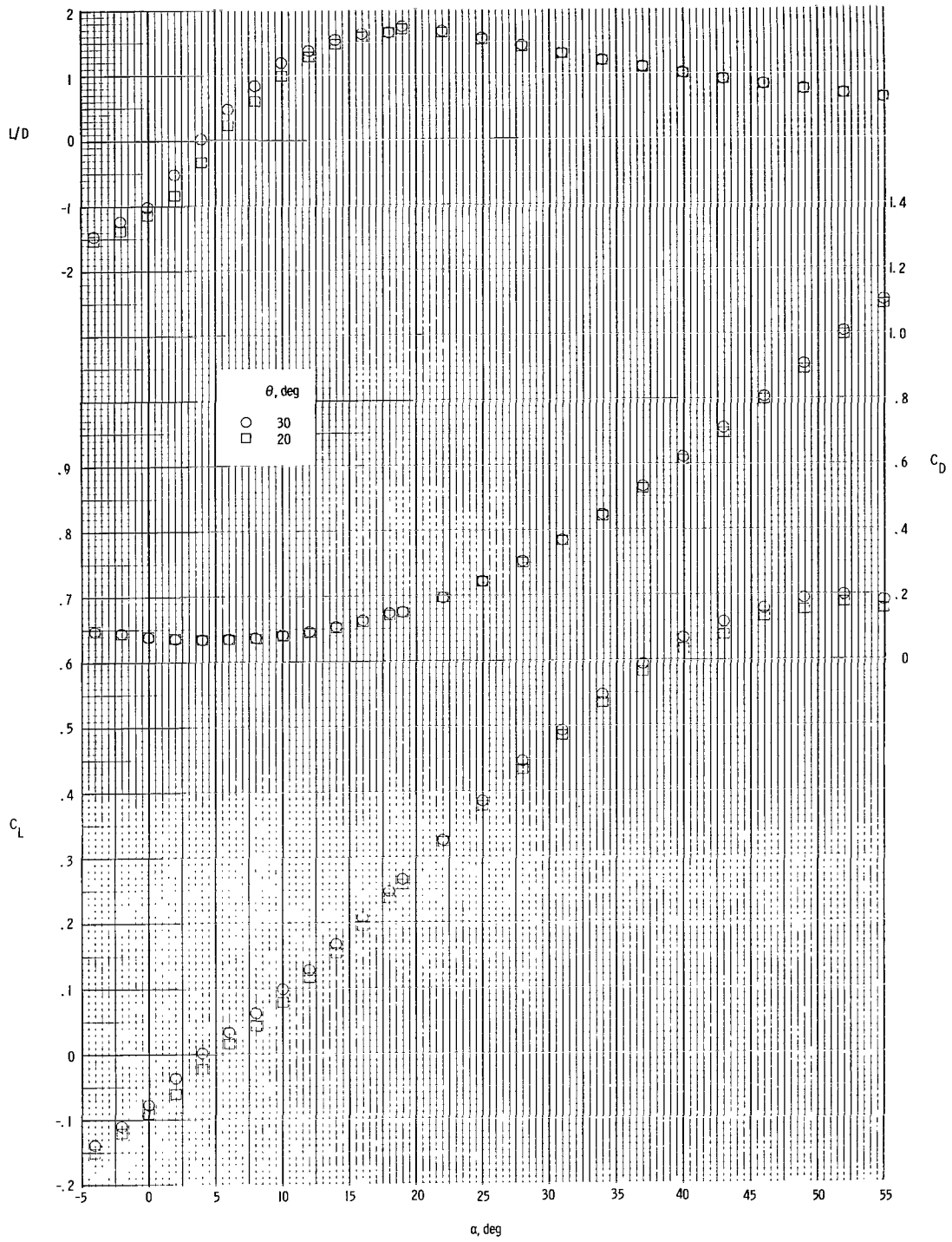


Figure 17.- Concluded.

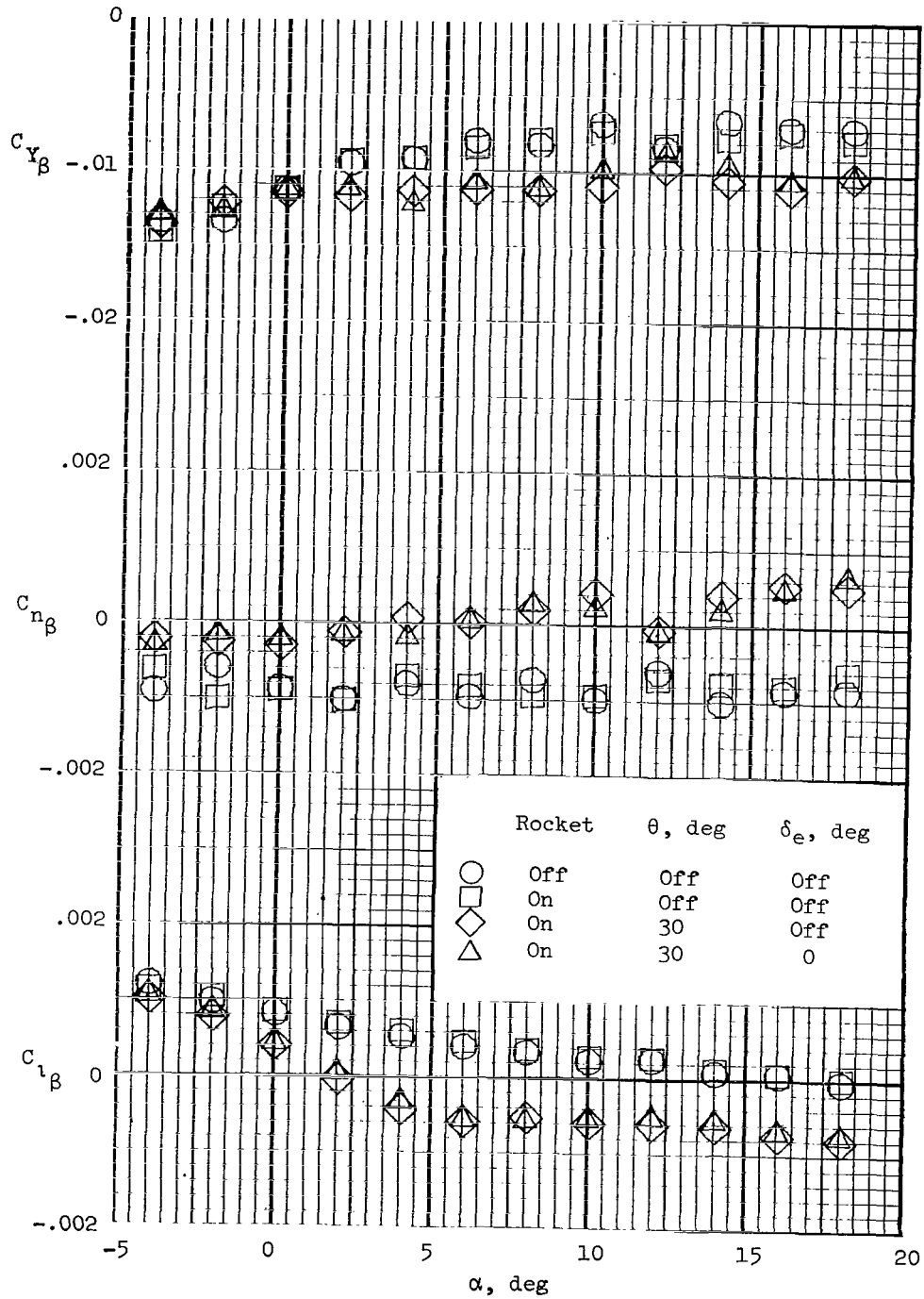


Figure 18.- Effect of configuration components on the lateral-directional characteristics of the lifting body at $M = 19$ and $R = 1.28 \times 10^6$.

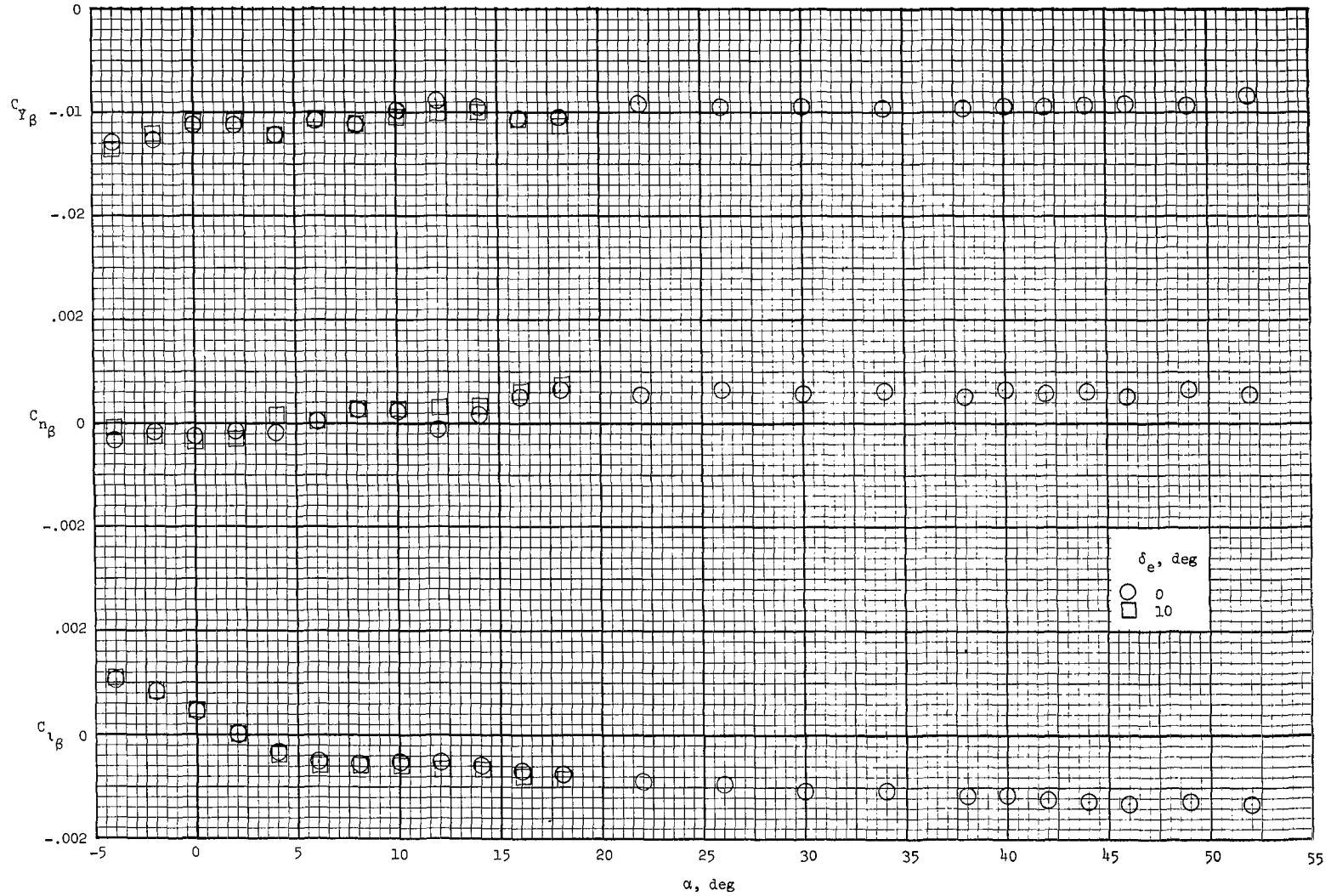


Figure 19.- Effect of longitudinal control on the lateral-directional characteristics of the lifting body with $\theta = 30^\circ$ at $M = 19$ and $R = 1.28 \times 10^6$.

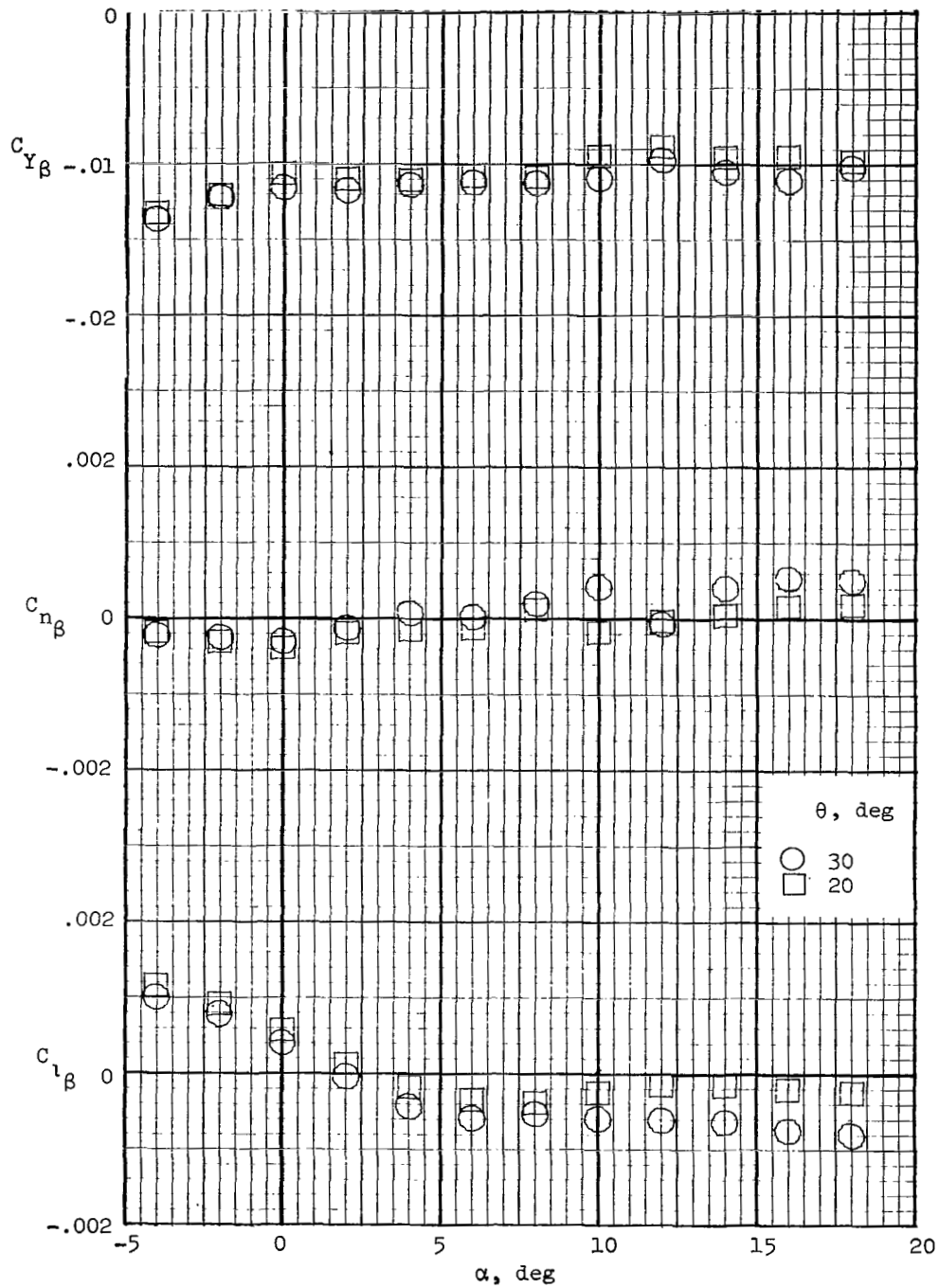


Figure 20.- Effect of tip-fin roll-out on the lateral-directional characteristics of the lifting body with δ_e off at $M = 19$ and $R = 1.28 \times 10^6$.

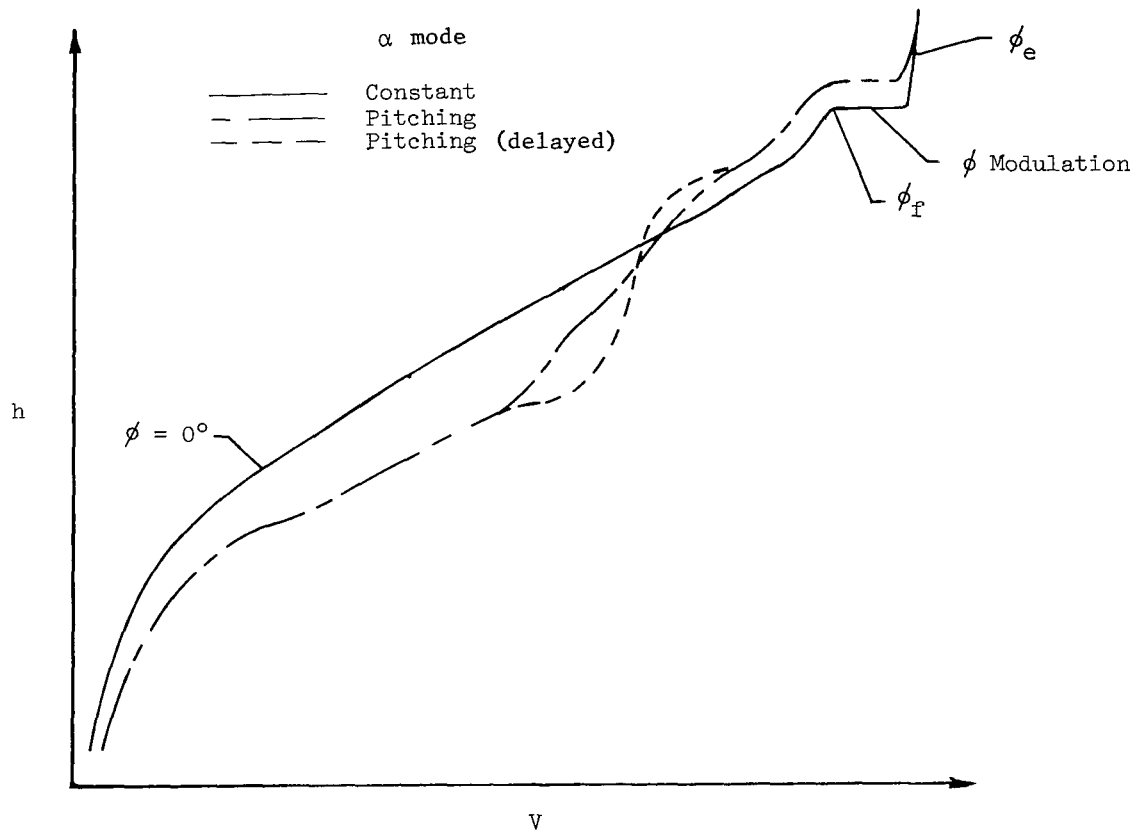
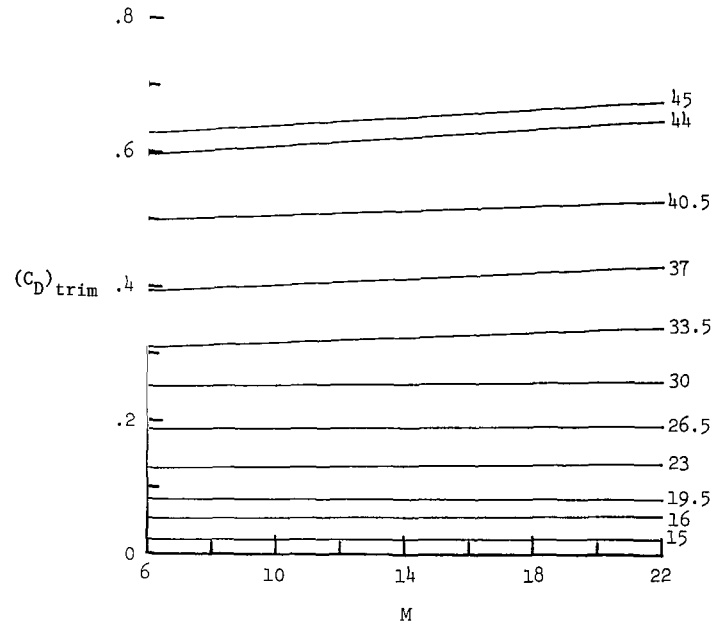
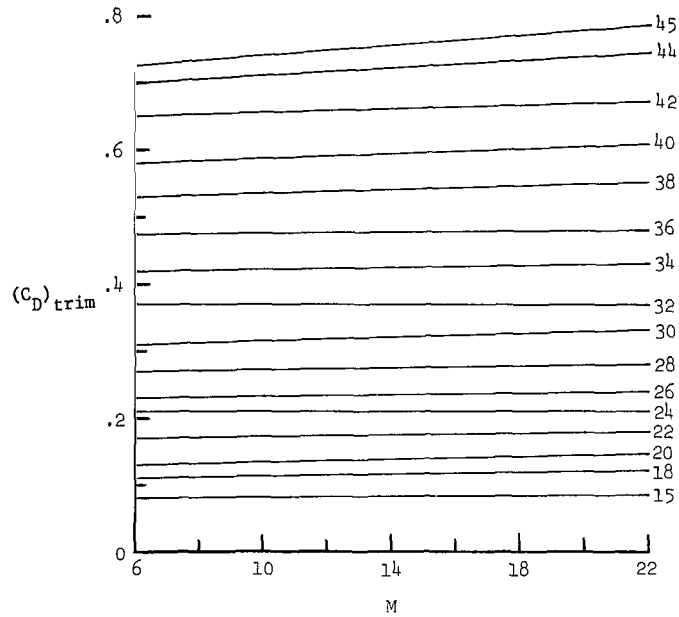
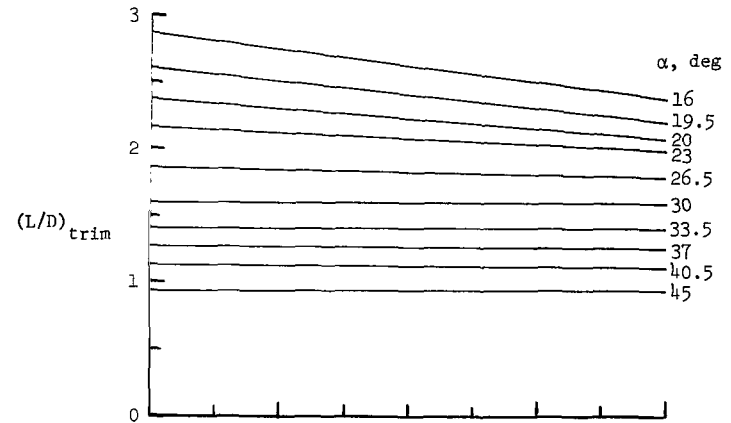
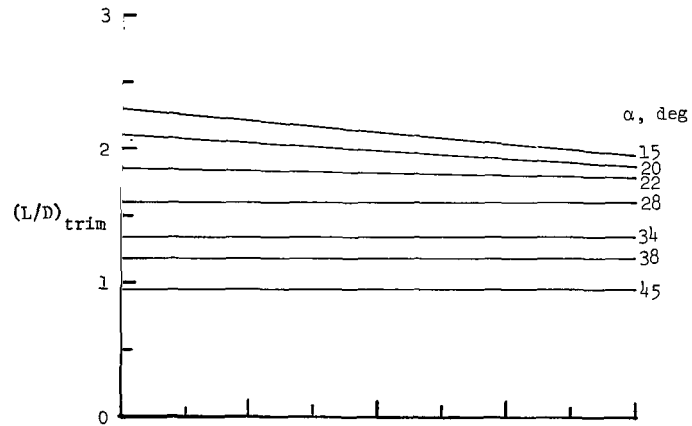


Figure 21.- Entry-mode comparison of typical trajectories.



(a) Experimental.

(b) Theoretical.

Figure 22.- Extrapolated wing-body data used in entry trajectory analysis.

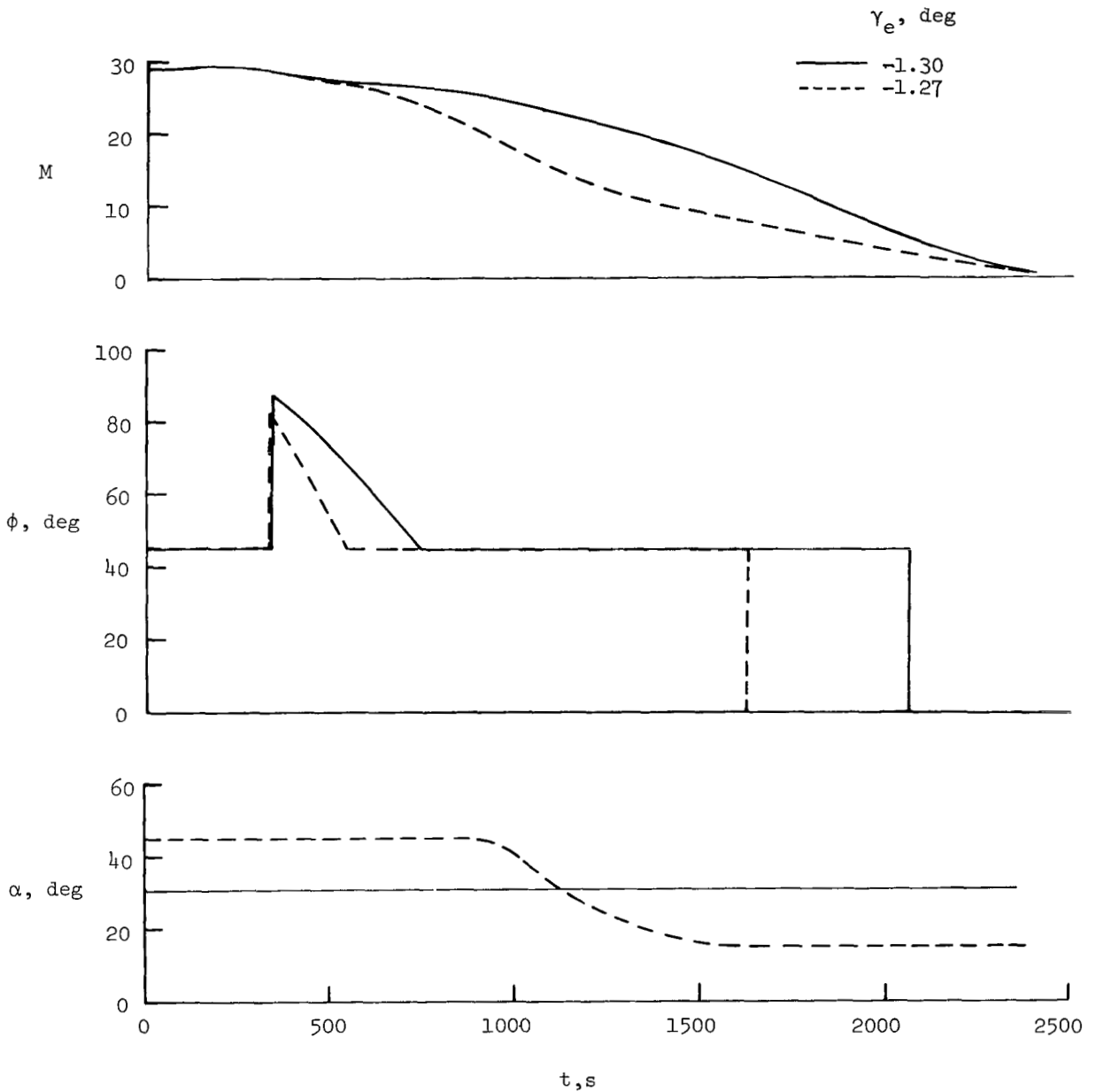


Figure 23.- Mach number, bank angle, and angle-of-attack variations for the wing-body orbiter during a 1500-n.-mi. cross-range entry using theoretical aerodynamics ($(L/D)_{\max} = 2.4$ at $M = 20$).

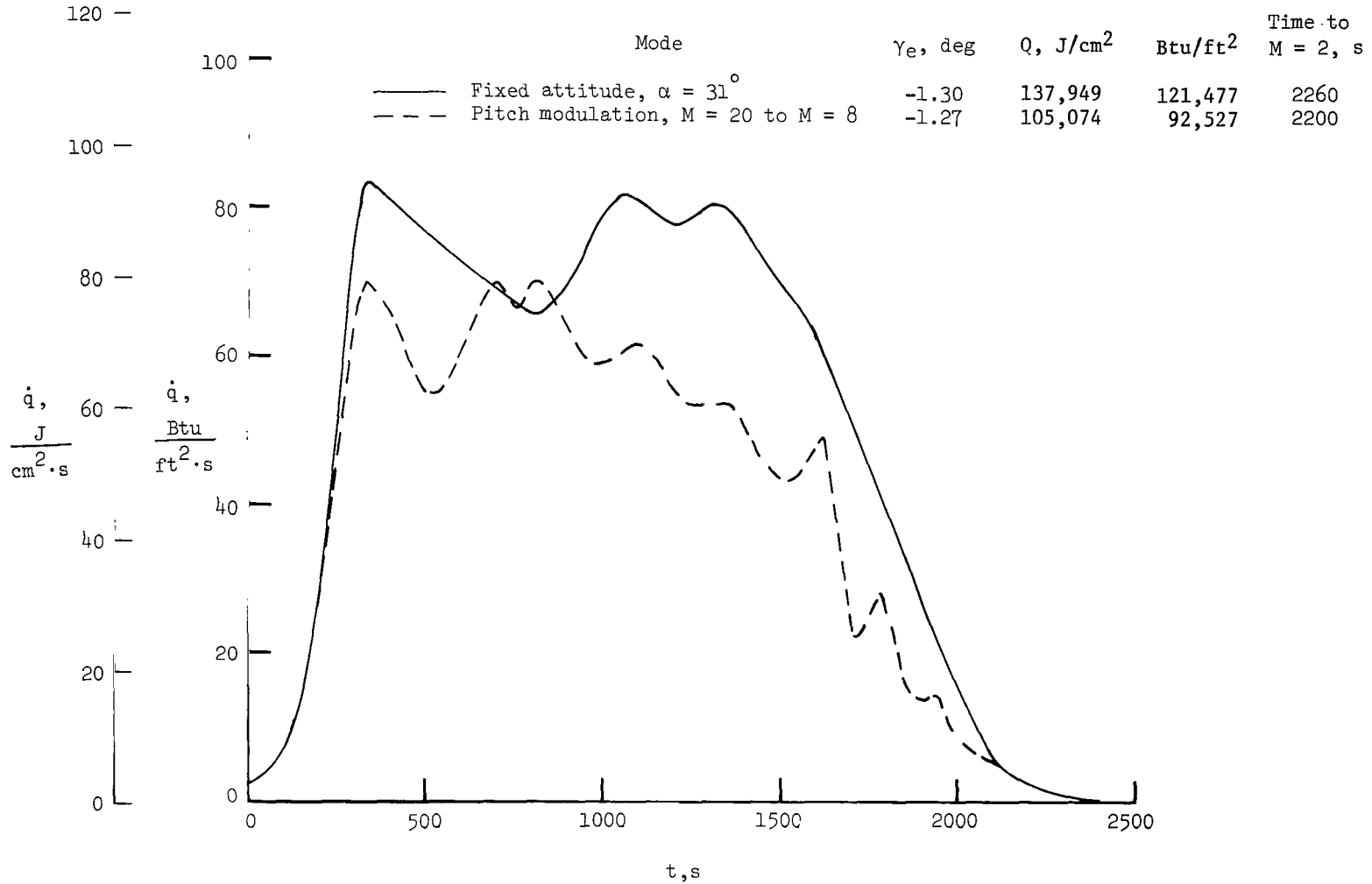


Figure 24.- Comparison of stagnation heating rates for 1500-n.-mi cross-range trajectories with $(L/D)_{\max} = 2.4$ at $M = 20$, $W/S = 1.77 \text{ kN/m}^2$ (37 psf), and based on a 0.305-meter-radius (1-ft) sphere.

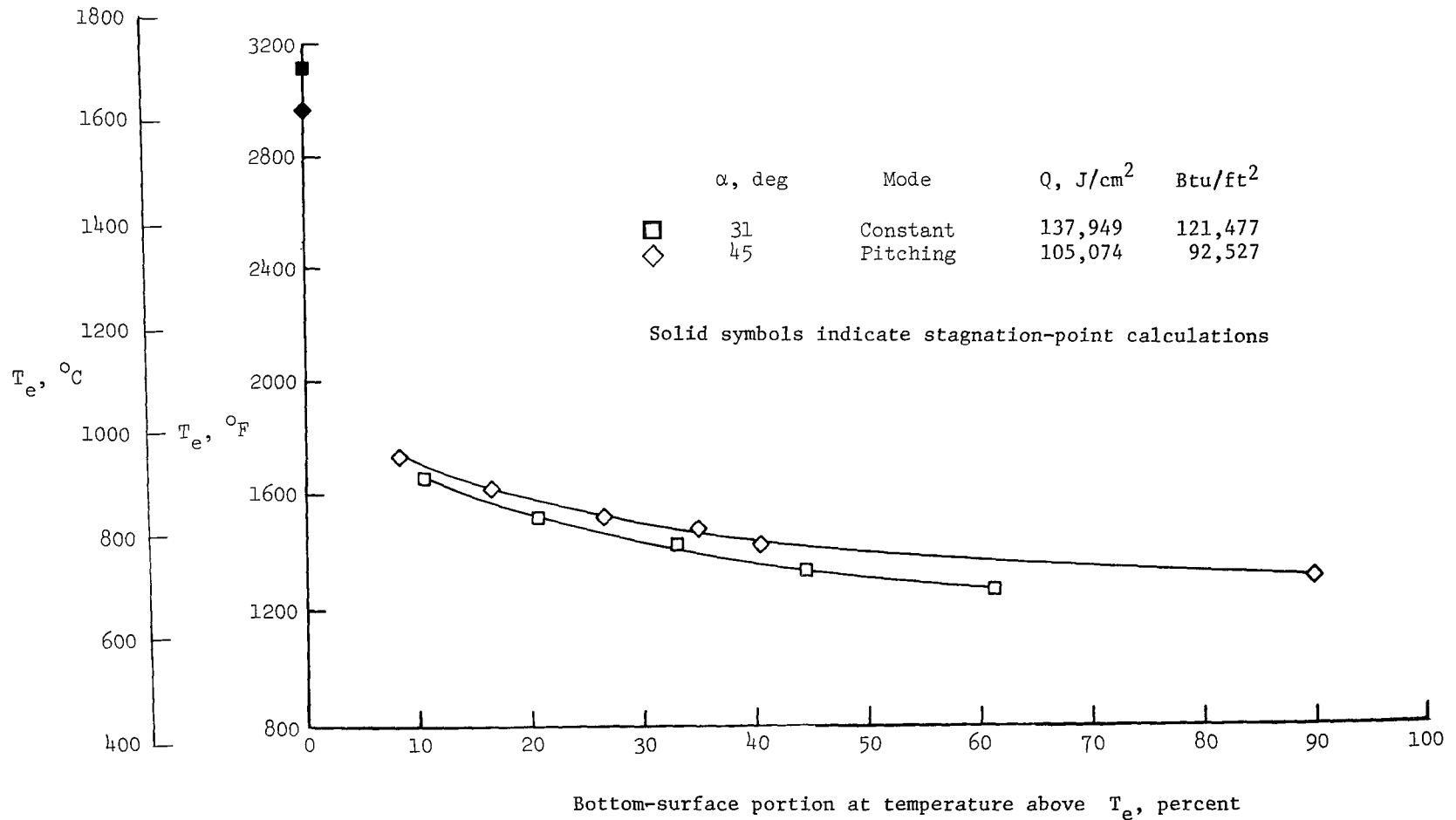
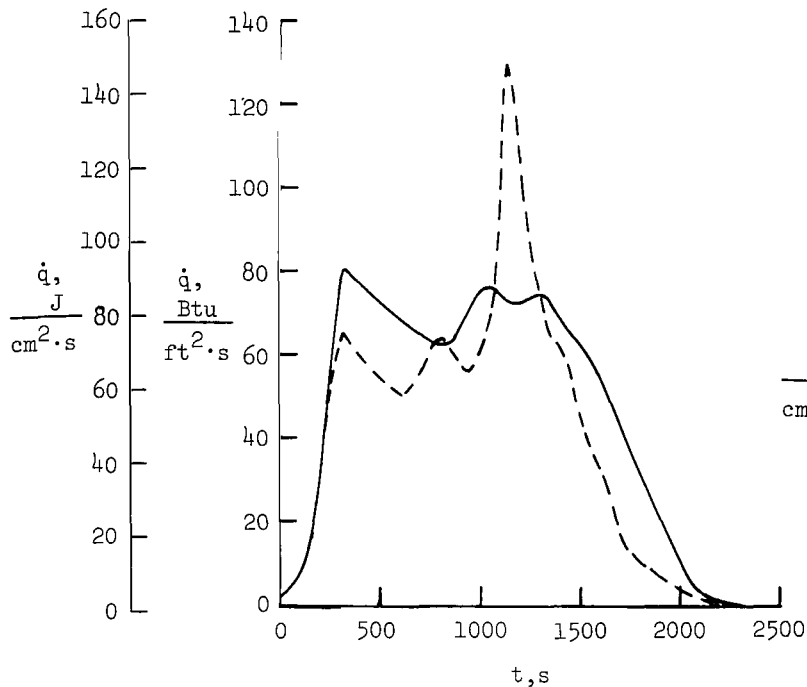
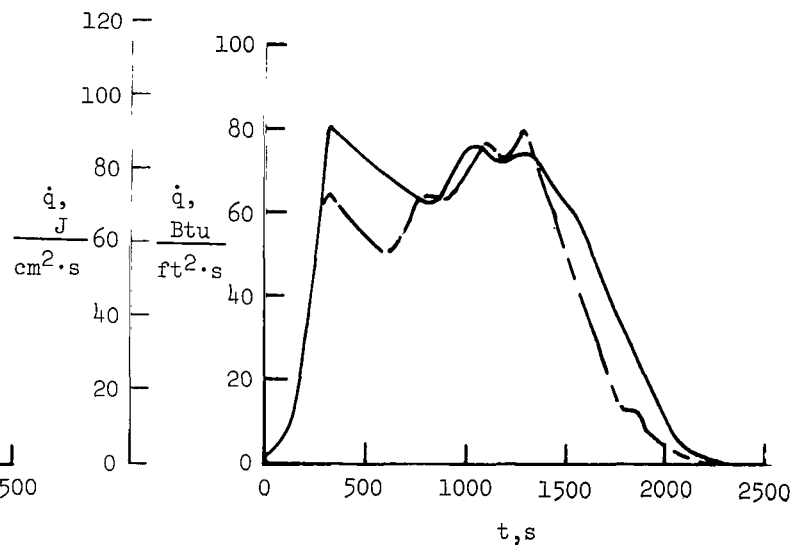


Figure 25.- Maximum-radiation equilibrium temperature on the lower surface of a delta-wing-body orbiter with an $(L/D)_{\max} = 2.4$ at $M = 20$, $W/S = 1.77 \text{ kN/m}^2$ (37 psf), nose radius of 0.53 m (1.75 ft), and an emissivity of 0.8. The cross range is 1500 n. mi.

Mode	γ_e , deg	Q , J/cm ²	Btu/ft ²	Time to M = 2, s
————— Constant, $\alpha = 29.6^\circ$	-1.32	127,698	112,450	2230
- - - - - Pitching, M = 20 to 16	-1.27	111,430	98,124	2110
- - - - - Pitching, M = 24 to 12	-1.27	109,907	96,783	2150



(a) Pitching, M = 20 to 16 compared with constant α .



(b) Pitching, M = 24 to 12 compared with constant α .

Figure 26.- Stagnation-heating-rate comparison of two variable-pitch entry modes with a constant α entry for a vehicle with an $(L/D)_{\max} = 2$ at M = 20 and $W/S = 1.77 \text{ kN/m}^2$ (37 psf). The cross range is 1500 n. mi. and the heating is based on a 0.305-meter-radius (1-ft) sphere.

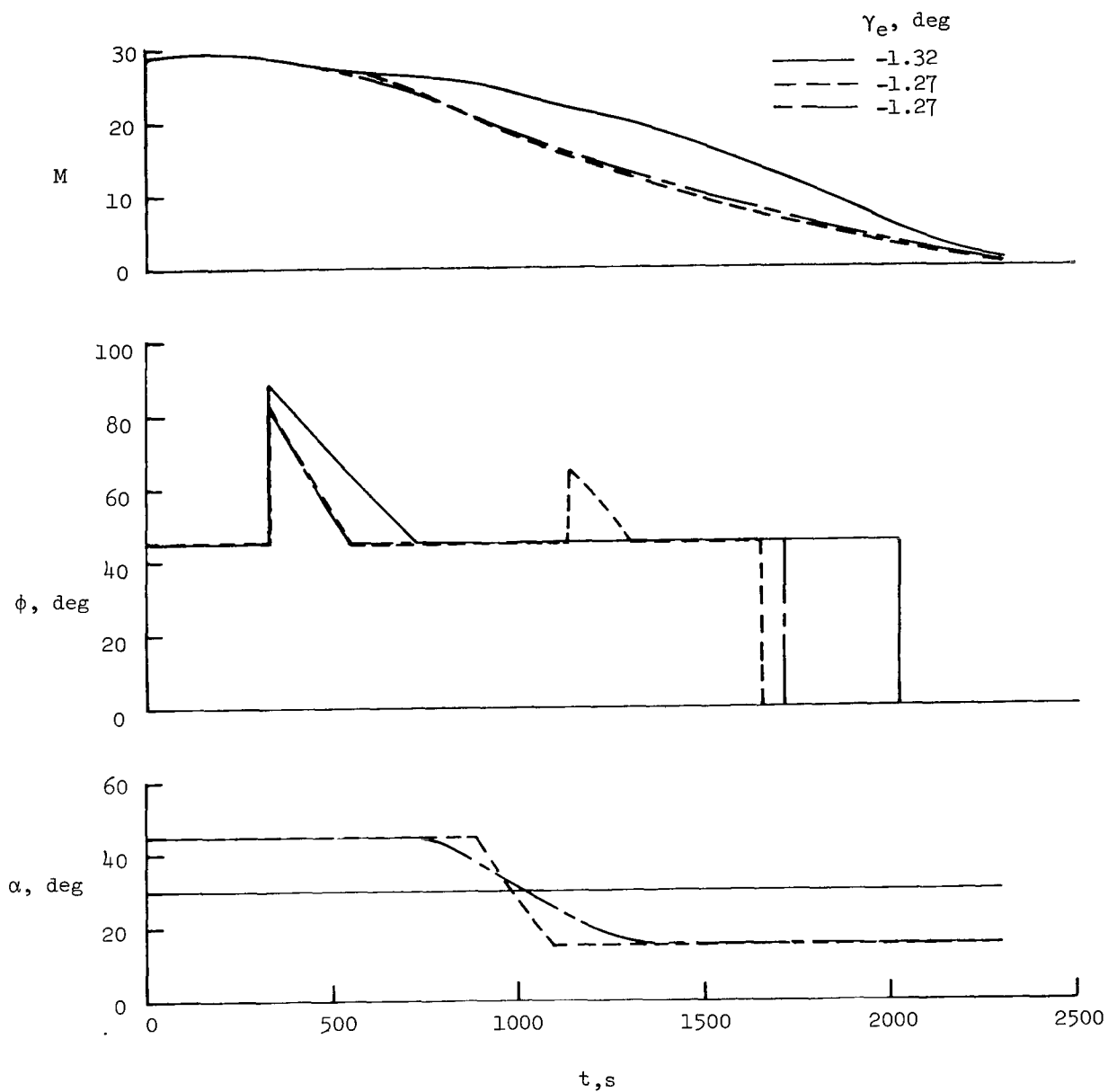


Figure 27.- Mach number, bank angle, and angle-of-attack variations for the wing-body orbiter during a 1500-n.-mi. cross-range entry using experimental aerodynamics ($(L/D)_{\max} = 2$ at $M = 20$).

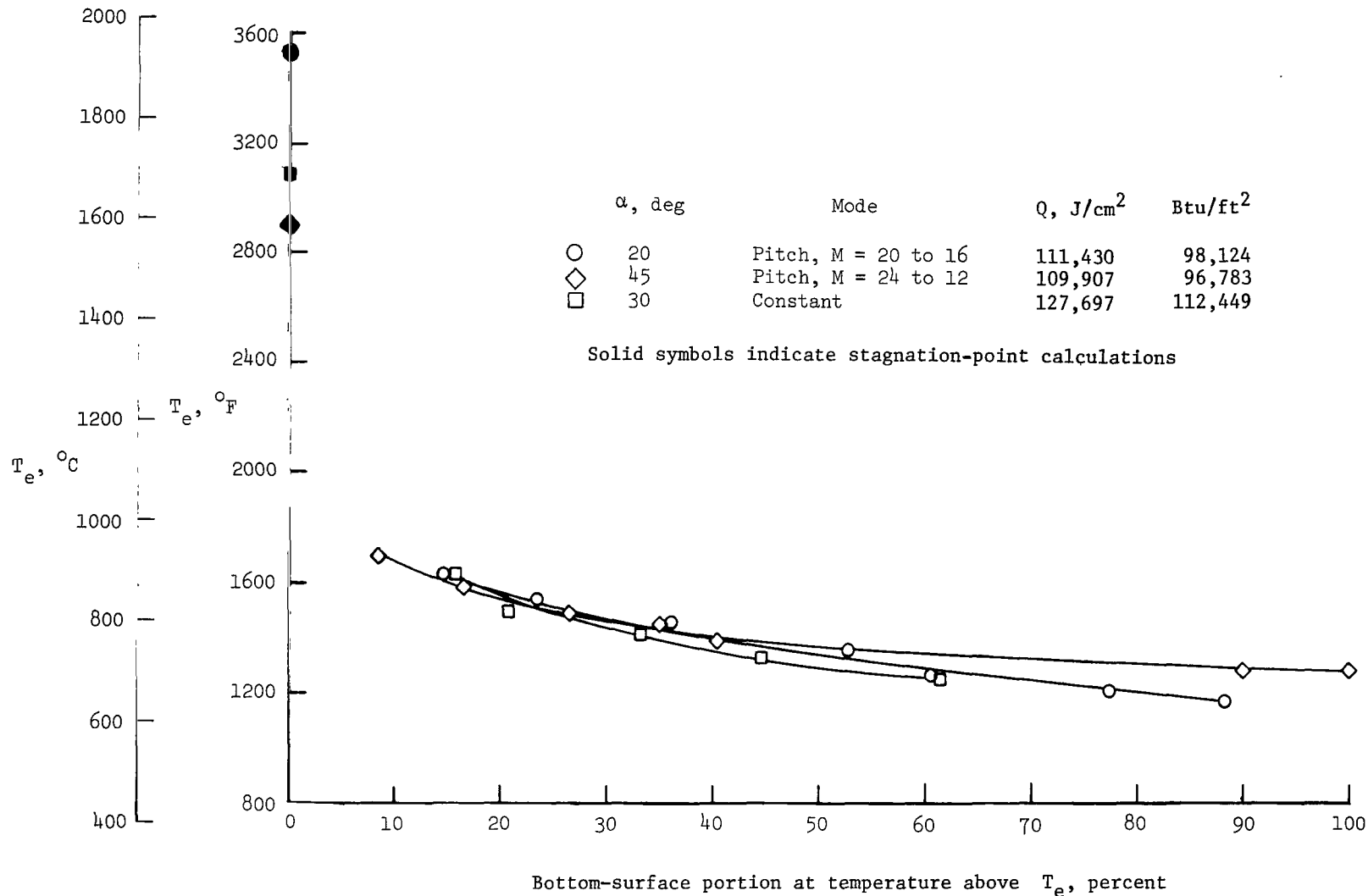
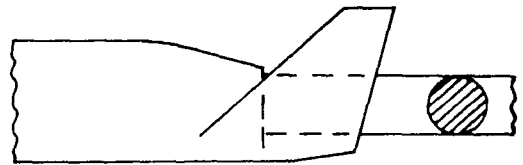
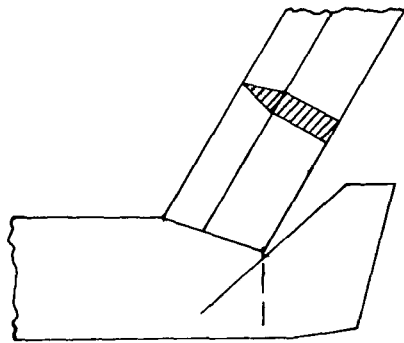
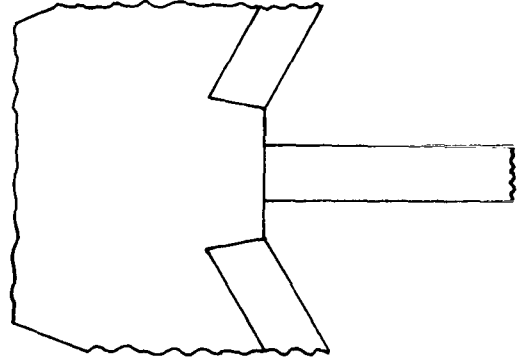
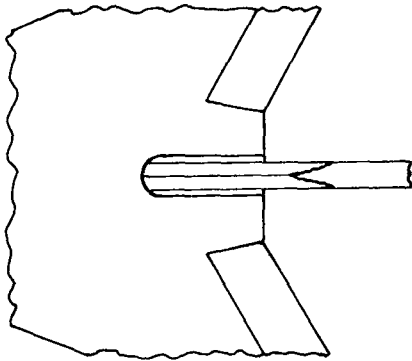


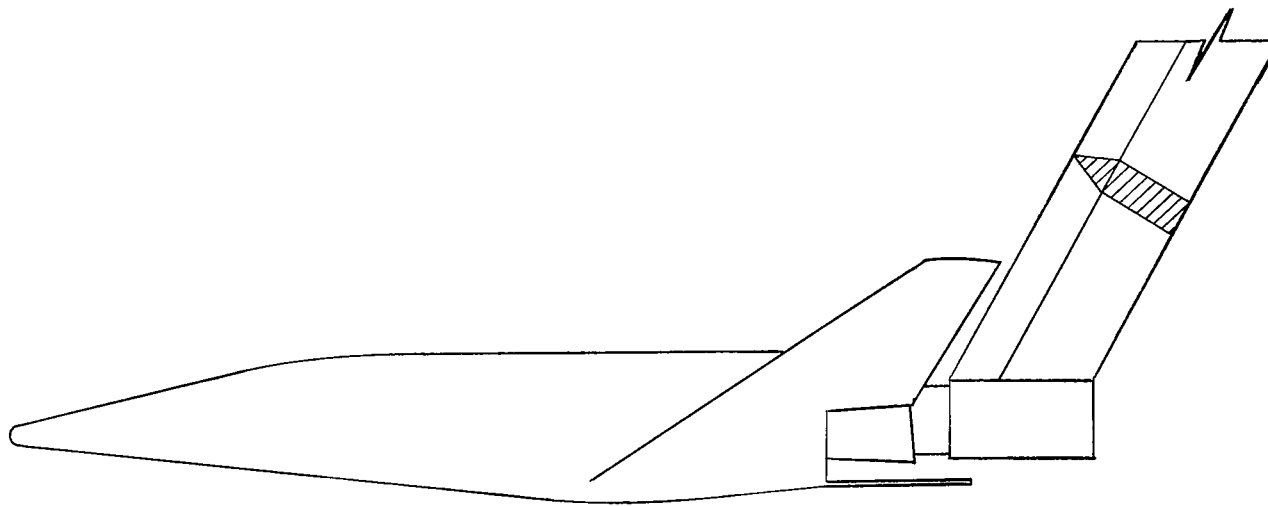
Figure 28.- Maximum-radiation equilibrium temperature on the lower surface of a delta-wing-body orbiter with an $(L/D)_{\text{max}} = 2$ at $M = 20$, $W/S = 1.77 \text{ kN/m}^2$ (37 psf), nose radius of 0.53 m (1.75 ft), and an emissivity of 0.8. The cross range is 1500 n. mi.



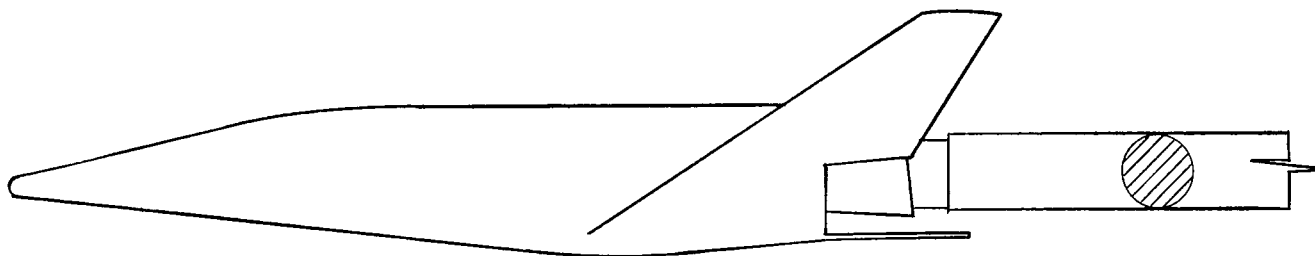
(a) Supported from top.

(b) Supported from base.

Figure 29.- Model-sting arrangements for the wing-body configuration.



(a) Dog-leg sting.



(b) Straight sting.

Figure 30.- Model-sting arrangements for the lifting-body configuration.

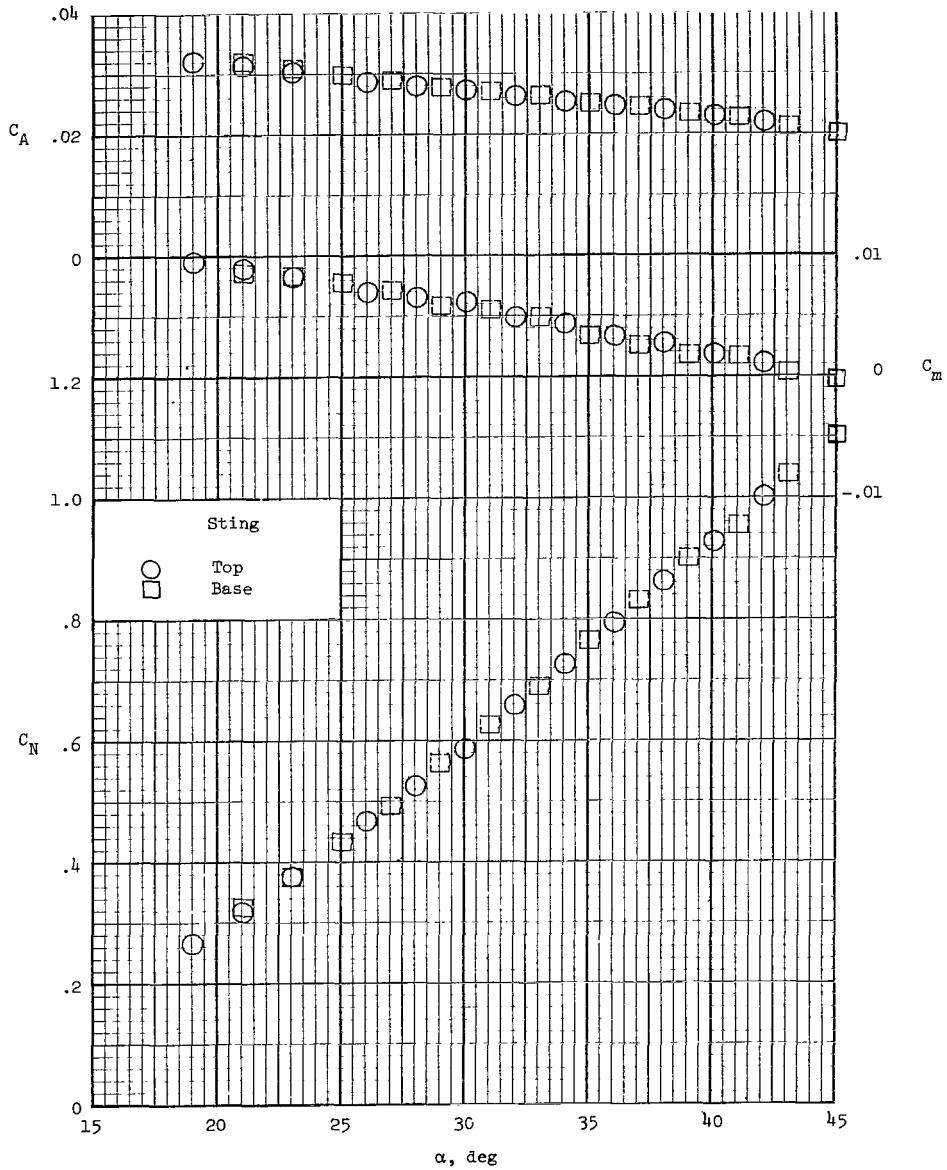


Figure 31.- Longitudinal aerodynamic characteristics for different model-sting arrangements of the wing-body configuration at $M = 20.6$ and $R = 3 \times 10^6$ for $\delta_e = -5^\circ$ and $\theta = 13.5^\circ$.

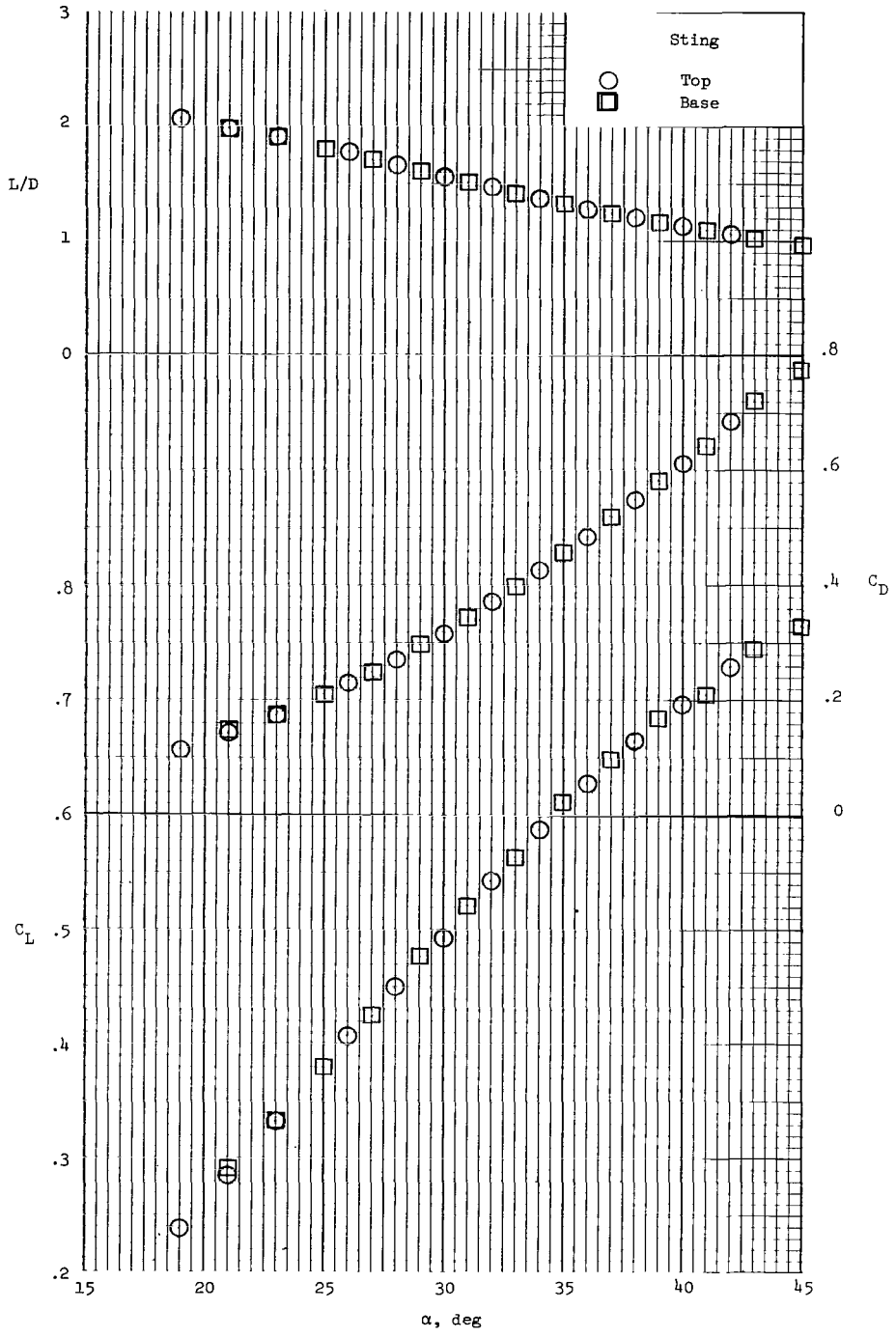


Figure 31.- Concluded.

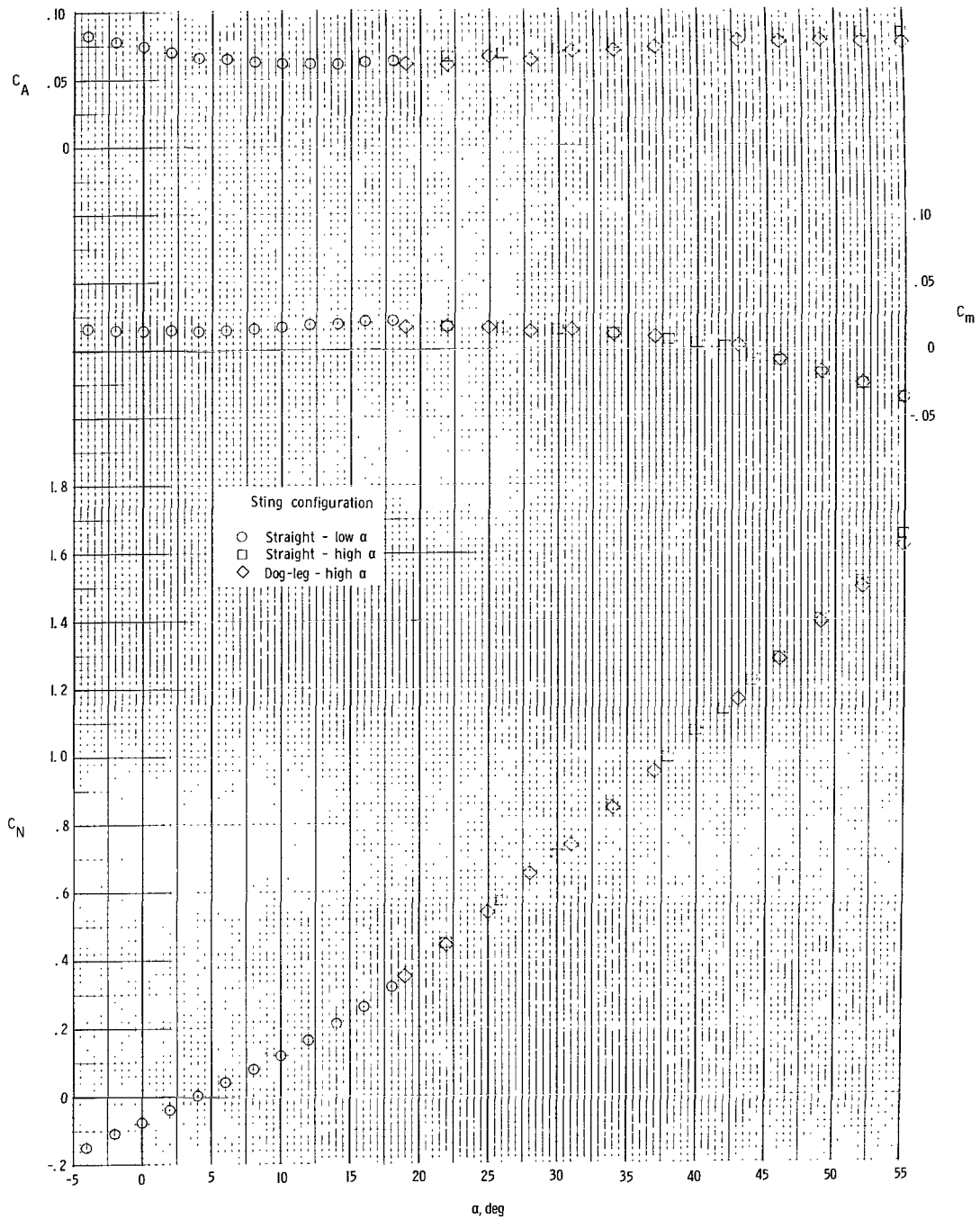


Figure 32.- Longitudinal aerodynamic characteristics for different model-sting arrangements of the lifting-body configuration with $\theta = 30^\circ$ at $M = 19$ and $R = 1.28 \times 10^6$.

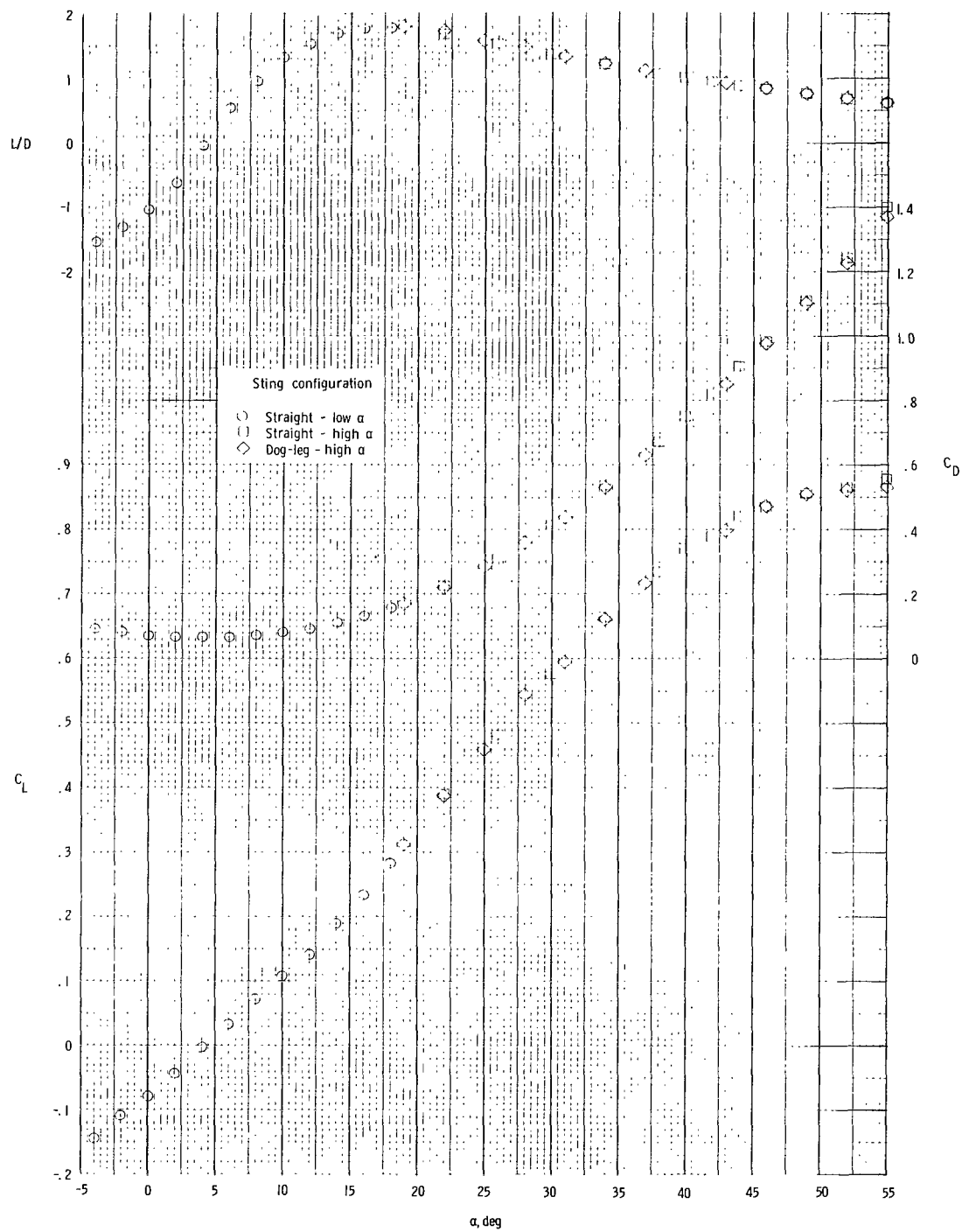


Figure 32.- Concluded.



016 001 C1 U 31 720414 S00903DS
DEPT OF THE AIR FORCE
AF WEAPONS LAB (AFSC)
TECH LIBRARY/WLOL/
ATTN: E LOU BOWMAN, CHIEF
KIRTLAND AFB NM 87117

POSTMASTER: If Undeliverable (Section 158
Postal Manual) Do Not Return

"The aeronautical and space activities of the United States shall be conducted so as to contribute . . . to the expansion of human knowledge of phenomena in the atmosphere and space. The Administration shall provide for the widest practicable and appropriate dissemination of information concerning its activities and the results thereof."

— NATIONAL AERONAUTICS AND SPACE ACT OF 1958

NASA SCIENTIFIC AND TECHNICAL PUBLICATIONS

TECHNICAL REPORTS: Scientific and technical information considered important, complete, and a lasting contribution to existing knowledge.

TECHNICAL NOTES: Information less broad in scope but nevertheless of importance as a contribution to existing knowledge.

TECHNICAL MEMORANDUMS: Information receiving limited distribution because of preliminary data, security classification, or other reasons.

CONTRACTOR REPORTS: Scientific and technical information generated under a NASA contract or grant and considered an important contribution to existing knowledge.

TECHNICAL TRANSLATIONS: Information published in a foreign language considered to merit NASA distribution in English.

SPECIAL PUBLICATIONS: Information derived from or of value to NASA activities. Publications include conference proceedings, monographs, data compilations, handbooks, sourcebooks, and special bibliographies.

TECHNOLOGY UTILIZATION PUBLICATIONS: Information on technology used by NASA that may be of particular interest in commercial and other non-aerospace applications. Publications include Tech Briefs, Technology Utilization Reports and Technology Surveys.

Details on the availability of these publications may be obtained from:

SCIENTIFIC AND TECHNICAL INFORMATION OFFICE

NATIONAL AERONAUTICS AND SPACE ADMINISTRATION

Washington, D.C. 20546